ARTICLES
https://doi.org/10.1038/s41591-019-0414-6
nature medicine

A longitudinal big data approach for precision health

Sophia Miryam Schüssler-Fiorenza Rose[1,2,3,16], Kévin Contrepois[1,16], Kegan J. Moneghetti[4,5,6], Wenyu Zhou[1], Tejaswini Mishra[1], Samson Mataraso[7,8], Orit Dagan-Rosenfeld[1], Ariel B. Ganz[1], Jessilyn Dunn[1,9], Daniel Hornburg[1], Shannon Rego[1], Dalia Perelman[1], Sara Ahadi[1], M. Reza Sailani[1], Yanjiao Zhou[10,11], Shana R. Leopold[10], Jieming Chen[12], Melanie Ashland[1], Jeffrey W. Christle[4,5], Monika Avina[1], Patricia Limcaoco[1], Camilo Ruiz[13], Marilyn Tan[14], Atul J. Butte[12], George M. Weinstock[10], George M. Slavich[15], Erica Sodergren[10], Tracey L. McLaughlin[14], Francois Haddad[4,5]* and Michael P. Snyder[1,4]*

Precision health relies on the ability to assess disease risk at an individual level, detect early preclinical conditions and initiate preventive strategies. Recent technological advances in omics and wearable monitoring enable deep molecular and physiological profiling and may provide important tools for precision health. We explored the ability of deep longitudinal profiling to make health-related discoveries, identify clinically relevant molecular pathways and affect behavior in a prospective longitudinal cohort ($n = 109$) enriched for risk of type 2 diabetes mellitus. The cohort underwent integrative personalized omics profiling from samples collected quarterly for up to 8 years (median, 2.8 years) using clinical measures and emerging technologies including genome, immunome, transcriptome, proteome, metabolome, microbiome and wearable monitoring. We discovered more than 67 clinically actionable health discoveries and identified multiple molecular pathways associated with metabolic, cardiovascular and oncologic pathophysiology. We developed prediction models for insulin resistance by using omics measurements, illustrating their potential to replace burdensome tests. Finally, study participation led the majority of participants to implement diet and exercise changes. Altogether, we conclude that deep longitudinal profiling can lead to actionable health discoveries and provide relevant information for precision health.

Precision health and medicine are entering a new era in which wearable sensors, omics technologies and computational methods have the potential to improve health and lead to mechanistic discoveries[1,2]. Emerging technologies such as longitudinal multi-omics profiling combined with clinical measures can comprehensively assess health and identify deviations from healthy baselines that may improve disease risk prediction and early detection. Connecting longitudinal multi-omics profiling with clinical assessment is also important for developing a new taxonomy of disease on the basis of molecular measures[1].

Despite this promise, few studies have leveraged emerging technologies and longitudinal profiling to manage health and identify disease markers. Previous efforts included our study of a single individual in which longitudinal multi-omics profiling over 14 months captured the individual's transition to diabetes on a deep molecular level[3]. A recent study of 108 individuals followed for 9 months using various omic technologies revealed several health-related findings[4]. A cross-sectional study used genome sequencing, metabolomics and advanced imaging to identify individuals at risk for age-related chronic disease[5]. These studies had limited sample size, lacked meaningful longitudinal profiling or performed only limited analysis of health information. We have also demonstrated the use of wearable devices to detect infections[2] and identify early glucose dysregulation[6] and population-based studies evaluating arrythmia detection are underway[7].

In the present study, we longitudinally profiled 109 participants at risk for diabetes mellitus (DM) (Fig. 1), performing quarterly clinical laboratory tests and multi-omics assessments. In addition, individuals underwent exercise testing, enhanced cardiovascular imaging and physiological testing, wearable sensor monitoring and completed various surveys.

The study objectives were three-fold. We first evaluated the usefulness of emerging technologies in combination with standard and enhanced clinical tests to detect diseases early. We then

[1]Department of Genetics, Stanford University School of Medicine, Stanford, CA, USA. [2]Spinal Cord Injury Service, Veteran Affairs Palo Alto Health Care System, Palo Alto, CA, USA. [3]Department of Neurosurgery, Stanford University School of Medicine, Stanford, CA, USA. [4]Stanford Cardiovascular Institute, Stanford University, Stanford, CA, USA. [5]Division of Cardiovascular Medicine, Department of Medicine, Stanford University School of Medicine, Stanford, CA, USA. [6]Department of Medicine, St Vincent's Hospital, University of Melbourne, Melbourne, Australia. [7]Department of Electrical Engineering and Computer Sciences, University of California, Berkeley, Berkeley, CA, USA. [8]Department of Bioengineering, University of California, Berkeley, Berkeley, CA, USA. [9]Mobilize Center, Stanford University, Stanford, CA, USA. [10]The Jackson Laboratory for Genomic Medicine, Farmington, CT, USA. [11]Department of Medicine, University of Connecticut Health, Farmington, CT, USA. [12]Bakar Computational Health Sciences Institute and Department of Pediatrics, University of California, San Francisco, CA, USA. [13]Department of Bioengineering, Stanford University, Stanford, CA, USA. [14]Division of Endocrinology, Stanford University School of Medicine, Stanford, CA, USA. [15]Cousins Center for Psychoneuroimmunology and Department of Psychiatry and Biobehavioral Sciences, University of California, Los Angeles, Los Angeles, CA, USA. [16]These authors contributed equally: Sophia Miryam Schüssler-Fiorenza Rose, Kévin Contrepois. *e-mail: fhaddad@stanford.edu; mpsnyder@stanford.edu

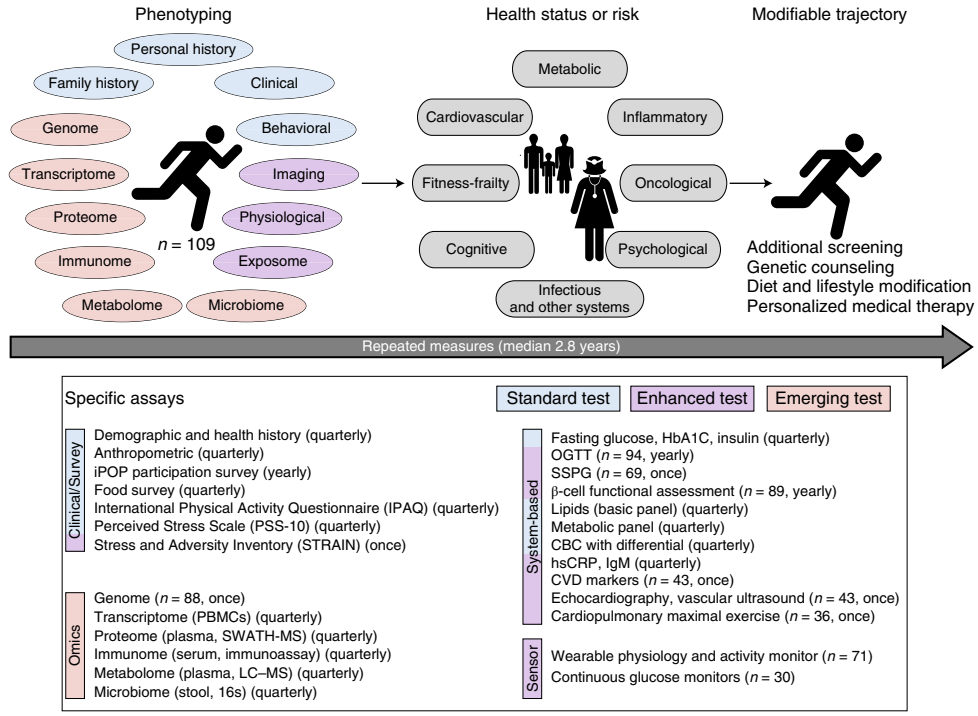

Fig. 1 | Study design and data collection. Overview of the in-depth longitudinal phenotyping used to determine health risk and status. Data types were categorized as: standard (blue), enhanced (purple) and emerging (red) tests. PBMCs, peripheral blood mononuclear cells; HbA1C, glycated hemoglobin; OGTT, oral glucose tolerance test; SSPG, steady-state plasma glucose; CBC, complete blood count; hsCRP, high sensitivity C-reactive protein; CVD, cardiovascular disease.

characterized multi-omics associations with clinical pathophysiologies including glucose and insulin dysregulation, inflammation and cardiovascular risk; we also evaluated the ability of multi-omics measures to predict insulin resistance and response to glucose load. Last, we examined how participation affected health habits.

Results

Summary of research design and cohort. A 109-person cohort enriched for individuals at risk for DM (Supplementary Table 1 and Extended Data Fig. 1a) underwent quarterly longitudinal profiling for up to 8 years (median 2.8 years) using standard and enhanced clinical measures and emerging assays. (Fig. 1). Emerging tests included molecular profiling of the genome, gene expression (transcriptome), proteins (proteome), immune proteins (immunome), small molecules (metabolome) and gut microbes (microbiome), and wearable monitoring including continuous glucose monitoring (CGM)[6]. Our study was designed to capture transitions from normoglycemic to pre-DM and from pre-DM to DM. Thus, in addition to standard measures such as fasting plasma glucose (FPG, reflects steady-state glucose metabolism[8]) and glycated hemoglobin (HbA1C, reflects 3-month average glucose), enhanced measures included the oral glucose tolerance test (OGTT, reflects response to glucose load[9]) with insulin secretion assessment (beta-cell function) and the modified insulin suppression test measuring steady-state plasma glucose (SSPG, a measure of peripheral insulin resistance). We also performed enhanced cardiovascular profiling including vascular ultrasound, echocardiography, cardiopulmonary exercise testing and cardiovascular disease protein markers. Technical details are provided in the methods and our integrated Human Microbiome Project (iHMP) paper[10]. The full details of the clinical laboratory measures, immune proteins and cardiovascular biomarkers are provided in Supplementary Table 0. The study was approved by the Stanford University Institutional Review Board (IRB 23602) and all participants consented.

The mean age of integrated personalized omics profiling (iPOP) participants at initial enrollment was 53.4 ± 9.2 years old. Demographic, baseline health and family history characteristics are shown in Supplementary Table 1. Genetic ancestry analysis ($n = 72$) using the 1,000 Genomes Project (1,000GP) data[11] shows that individuals mapped to expected ancestral populations (Extended Data Fig. 1b).

Over the study course, we found over 67 major clinically actionable health discoveries spanning metabolism, cardiovascular disease, oncology and hematology, and infectious disease (Supplementary Table 2). We demonstrate ways in which longitudinal multi-omics measures can be used to advance precision health, including by illuminating biological pathways underlying standard measures, predicting burdensome physiological measurements and enabling exploration of mechanisms of disease onset.

Metabolic health profiling. At entry, participants reported their DM status. Of the 86 participants (78.9%) who did not report pre-DM or DM, one had a diagnosis of DM in their health record, one had a DM-range HbA1C and 43 individuals (39.4%) had laboratory results in the pre-DM range at entry (Fig. 2a). During the study, eight more individuals converted to DM as assessed by a clinical diagnosis of DM ($n = 4$), starting a diabetic medication after a diabetic-range laboratory result ($n = 3$), and/or if they had laboratory results in the diabetic range ($n = 6$) at more than one time point. Five additional participants developed laboratory abnormalities in the diabetic range at one time point, and 12 developed abnormalities in the prediabetic range. In addition, two participants had diabetic-range CGM measurements (>2 mg ml^{-1}) who were normoglycemic on FPG, HbA1C and OGTT (Supplementary Table 3) indicating that these individuals have glucose dysregulation that is most easily assessed using CGM.

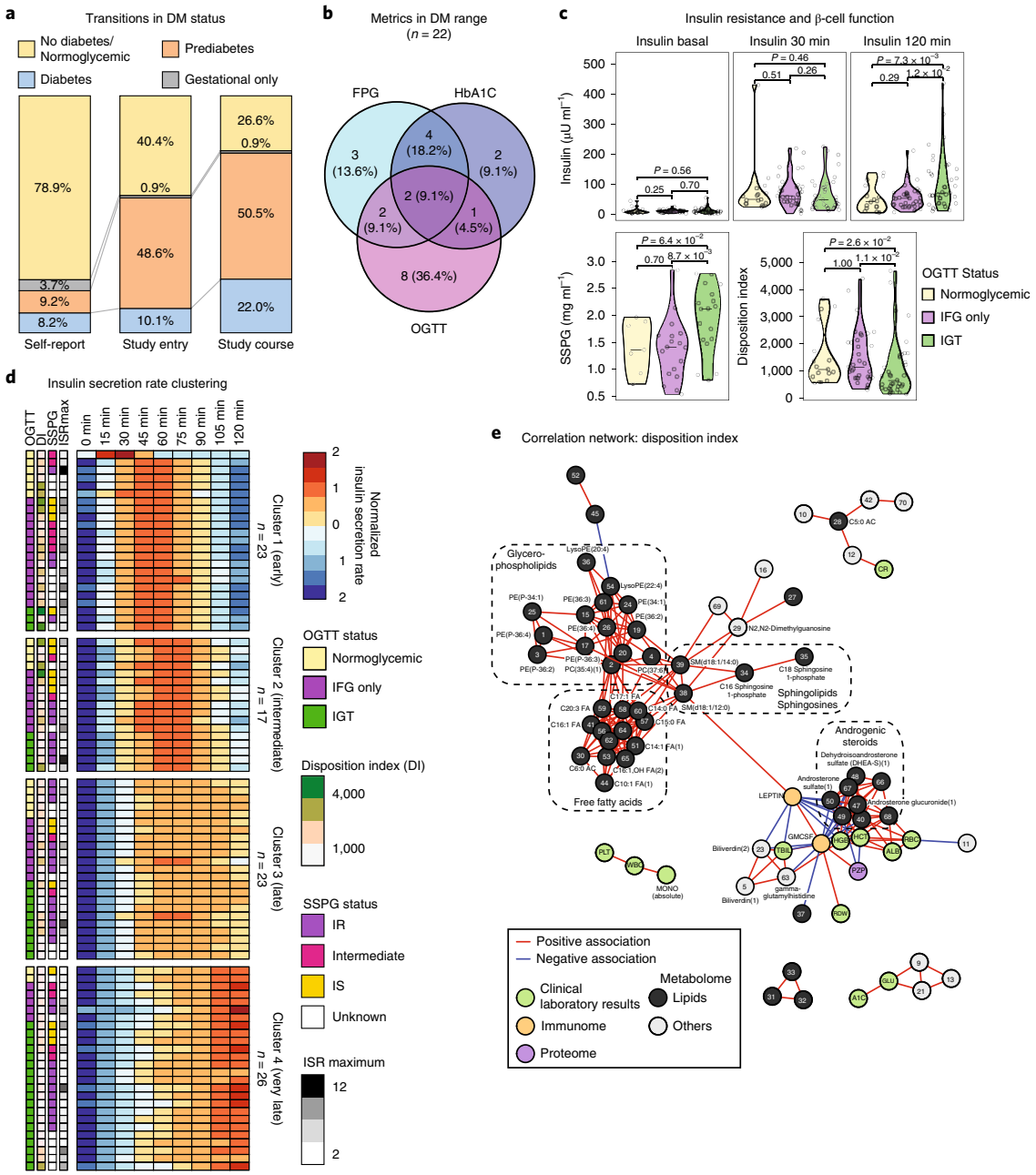

Fig. 2 | Clinical and enhanced phenotyping of glucose metabolism, insulin production and resistance. a, Transitions in DM status ($n = 109$). First column, self-reported DM status. Second column, DM status determined by self-report; medical records and study entry diabetes-related laboratory measures: FPG, HbA1C and OGTT; prediabetic range (1.0 mg ml^{-1} ≤ FPG < 1.26 mg ml^{-1} or 5.7% ≤ HbA1C < 6.5% or 1.4 mg ml^{-1} ≤ OGTT < 2.0 mg ml^{-1}); diabetic range (FPG ≥ 1.26 mg ml^{-1} or HbA1C ≥ 6.5% or OGTT (2-h) ≥ 2.0 mg ml^{-1}). Third column, DM history and status determined by the initial report and diabetes-related laboratory measures over the course of the study. For FPG to be considered impaired or diabetic, two values in these ranges were required over the course of the study, whereas for HbA1C and OGTT only one value was required. **b**, Overlap of diabetic-range laboratory results by participants over the course of the study. Diabetic ranges are as in panel **a**. **c**, Violin plots showing insulin levels during OGTT at 0, 30 and 120 min, SSPG ($n = 43$ participants) and glucose disposition index ($n = 89$ samples from 61 participants) by glycemic status determined by OGTT including normoglycemic, impaired fasting glucose only (IFG only: FPG ≥ 1.0 mg ml^{-1}), and impaired glucose tolerance (IGT: OGTT ≥ 1.4 mg ml^{-1}). SSPG was measured using the modified insulin suppression test. The disposition index was calculated as the insulin secretion rate (ISR) at 30 min times the Matsuda index ((pmol kg^{-1} min^{-1}/(mg ml^{-1} × μU ml^{-1})). A two-sided Wilcoxon *t*-test was used for differential analysis. The violin plots illustrate kernel probability density (that is, the width represents the proportion of the data) and the horizontal bar depicts the median of the distribution. **d**, Heat map showing ISRs that were row standardized and clustered using *k*-means clustering ($n = 89$ samples from 61 participants). Observations in clusters were ordered by OGTT status. OGTT status, disposition index (DI), SSPG (insulin sensitive (IS), SSPG < 1.00 mg ml^{-1}; intermediate, 1.00 mg ml^{-1} ≤ SSPG < 1.50 mg ml^{-1}; insulin resistant (IR), SSPG ≥ 1.50 mg ml^{-1}) and maximum insulin secretion rate (ISR maximum) are indicated on the left-hand side of the heat map. **e**, Correlation network of multi-omics measures associated with the glucose disposition index ($n = 89$ samples from 61 participants; Benjamini–Hochberg false discover rate (FDR) < 0.1). Correlations were calculated using Spearman correlation and considered significant if Bonferroni-corrected $P < 0.05$. Only networks containing a minimum of three molecules were plotted.

Value of exome sequencing. Exome sequencing[12] provided relevant information for diabetes management. Most notable was the discovery of a *HNF1A* mutation, pathogenic for maturity-onset diabetes of the young (MODY), in a participant with DM. This discovery has implications for medications[13] and the individual decided to have their children tested. It was valuable to exclude a MODY mutation in a second participant with a DM history concerning for MODY. Other discoveries are listed in Supplementary Table 2.

Enhanced metabolic profiling. DM is a complex disease with various underlying pathophysiologies including insulin resistance, pancreatic beta-cell dysfunction and abnormal gluconeogenesis[14], which can have differential effects on standard measures. Over the course of the study, 22 participants had at least one test result in the diabetic range (Fig. 2b) but few ($n=2$) had concordance of all three measures. When performed simultaneously, FPG-HbA1C and FPG-OGTT were in agreement 65.2% and 52.6% of the time, respectively (Extended Data Fig. 2a,b), highlighting that DM status varies depending on the assessment method. Most participants also underwent insulin sensitivity assessment ($n=69$); 55% were resistant (SSPG $\geq 1.5\,mg\,ml^{-1}$). In addition, insulin secretion during OGTT was assessed in 61 participants using the C-peptide deconvolution method[15] and the glucose disposition index was calculated[16]. On the basis of OGTT measurements, participants were categorized into three groups: normoglycemic, impaired fasting glucose only (IFG only) and impaired glucose tolerance (IGT). We observed large inter-individual variability in insulin levels, insulin resistance and disposition index between groups (Fig. 2c). Participants with IGT had higher insulin levels 120 min post-OGTT test, higher SSPG (more insulin resistant) and a lower disposition index. Cluster analysis of the longitudinal pattern of insulin secretion rates (ISRs) during OGTTs demonstrated four insulin secretion groups: early, intermediate, late and very late (Fig. 2d). Each cluster was heterogeneous in terms of OGTT status, disposition index, insulin resistance status and maximum insulin level and demonstrated no consistent pattern of molecular enrichment, indicating high heterogeneity in glucose dysregulation.

We also searched for multi-omics molecular associations with the disposition index across the cohort and found 109 significant molecules (FDR < 0.1) (Supplementary Table 4). HbA1C (FDR $= 2.0\times10^{-3}$) and FPG (FDR $= 4.9\times10^{-2}$) were negatively associated with disposition index as expected from previous reports showing increased FPG and HbA1C with beta-cell dysfunction[17,18]. We found that disposition index was strongly negatively associated with leptin (FDR $= 1.6\times10^{-7}$) and GM-CSF (FDR $= 7.2\times10^{-7}$), which are known regulators of energy homeostasis and inflammation signaling[19,20]. GM-CSF (FDR $= 1.5\times10^{-7}$) and leptin (FDR $= 3.3\times10^{-7}$) were also the two analytes that were most strongly positively associated with body mass index in our cohort and were positively associated with hsCRP illustrating their connection to inflammation and obesity. In the disposition index correlation network, leptin and GM-CSF were correlated with various lipid classes including an inverse correlation with androgenic steroids, and a positive correlation with sphingolipids and sphingosines, free fatty acids and glycerophospholipids highlighting their importance in lipid metabolism[21] (Fig. 2e and Supplementary Table 5).

Longitudinal course and mechanistic insights. A study strength is its dense longitudinal sampling approximately every 3 months. On the basis of individual longitudinal HbA1C trajectories, participants were classified into six categories (Extended Data Fig. 2c). Notably, it was common for participants' HbA1C to alternate between the normal–pre-DM ($n=21$) and pre-DM–DM ranges ($n=8$). No one stayed exclusively in the DM range due to good diabetes control with lifestyle and medications. Consistent transitions from normal to pre-DM ($n=5$) and from pre-DM to normal HbA1C ($n=10$) were overall less common.

Close evaluation of individual trajectories of participants with new diabetes ($n=9$) revealed additional insights. Individual trajectory analysis revealed that participants followed multiple pathways to diabetes (Fig. 3a–c, Extended Data Fig. 3 and Supplementary Table 3). Some participants' ($n=2$) first abnormality was DM-range OGTT (Fig. 3a and Extended Data Fig. 3a), others ($n=3$) had elevated FPG (Fig. 3b and Extended Data Fig. 3b,c) and the remainder ($n=4$) had a DM-range HbA1C (Extended Data Fig. 3d,e) or abnormalities in multiple measures (Fig. 3c and Extended Data Fig. 3f). Diabetic-range laboratory results followed viral infections[3] in one participant (Fig. 3c). Also, one participant with a single DM laboratory result improved their SSPG with diet and exercise (Extended Data Fig. 3g) and never had a second DM-range laboratory result during the study.

Progression to DM was associated with weight gain and decreased gut microbiome diversity (Shannon) in two out of eight participants (Fig. 3a,b and Extended Data Fig. 4a,b). In both cases, the phylum Bacteroidetes proportion was increased at the time point of lowest diversity to the detriment of beneficial bacteria such as the genus faecalibacterium (Extended Data Fig. 4c–e). Using linear mixed models to account for repeated measures, we evaluated the relationships between microbiome diversity and SSPG, FPG and HbA1C and found an inverse relationship with diversity that was strongest with SSPG ($P=1.5\times10^{-4}$) (Supplementary Table 6). We then performed longitudinal mixed model analysis to understand changes in diversity over time (Supplementary Table 7). SSPG accounted for 28% of the between-person Shannon variance highlighting the importance of insulin resistance in microbiome diversity. The majority of Shannon variance was intra-individual (76.8%) and adding the Bacteroidetes phylum proportion to the model including its interaction with time accounted for 41% of the remaining within-person variance, consistent with the relationship observed in the individual profiles between Bacteroidetes proportion and diversity.

Longitudinal evaluation of all data related to glucose and insulin regulation provided insights into mechanism. For instance, the person in Fig. 3c had a normal SSPG despite a diabetic-range OGTT, FPG and HbA1c. Although elevated OGTT is commonly thought to result from increased peripheral resistance or decreased insulin production, this participant had elevated insulin production with a delayed response trajectory, possibly reflecting delayed insulin release (Supplementary Table 3). Other mechanistic insights are provided in Supplementary Table 3. In conclusion, participants developed diabetes through different pathways, and our detailed characterization provides potential hypotheses regarding individual underlying mechanisms of glucose dysregulation, which is a goal of precision medicine.

Multi-omic dimensions of glucose metabolism and inflammation. We examined the underlying relationships between glucose (FPG, HbA1C) and inflammation (hsCRP) levels and multi-omics measurements at healthy time points (healthy-baseline models) and with relative changes for all time points (dynamic models) using linear mixed models. The two analyses are complementary since the healthy-baseline models highlight the stable relationships between measures and dynamic models highlight common associations with change.

As expected, the healthy-baseline analysis demonstrated that HbA1C and FPG strongly associated with each other and the 'glucose homeostasis' pathway (Fig. 3d, Extended Data Fig. 5 and Supplementary Tables 8–13). Although the two measures had many common associations, particularly with metabolites including lipids (free fatty acids and total triglyceride level (TGL)) and amino acids as previously reported[22], many analytes were exclusively associated with FPG or HbA1C, highlighting the differential underlying biology captured by both measures. While HbA1C associated with

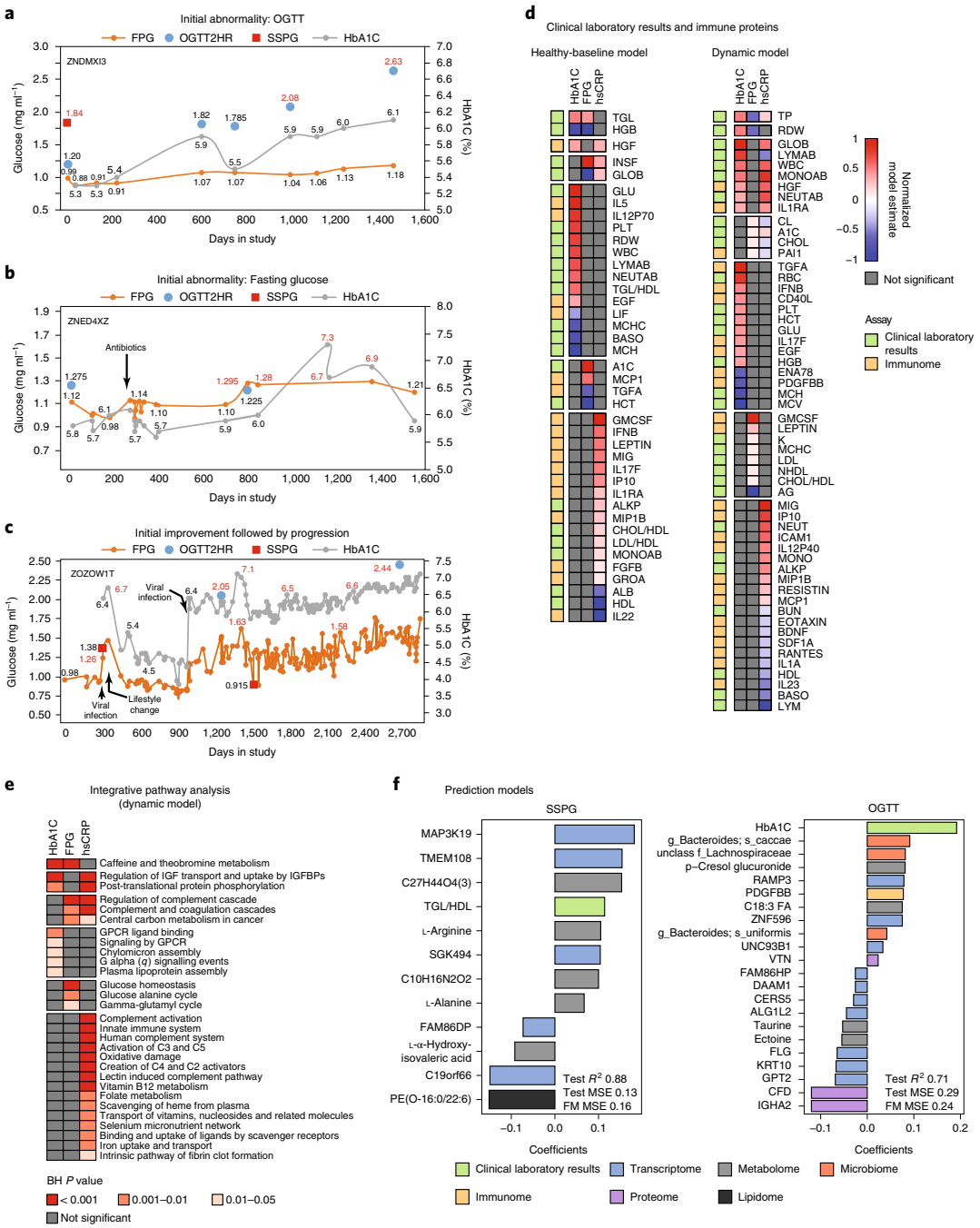

Fig. 3 | Longitudinal individual phenotyping and multi-omics of glucose metabolism and inflammation. a–c, Longitudinal diabetic measures demonstrating different patterns of DM onset and progression with initial abnormality response to glucose load (OGTT) (**a**), initial abnormality in fasting glucose metabolism (FPG) (**b**) and initial improvement followed by progression (**c**). Diabetic-range metrics are indicated in red. **d**, Clinical markers and immune proteins associated with HbA1C, FPG and hsCRP using healthy-baseline and dynamic models. Healthy-baseline models are linear mixed models that take into account repetitive measures across participants (HbA1C $n=101$, samples 560; FPG $n=101$, samples 563; hsCRP $n=98$, samples 518). Dynamic models are similar models except that analytes are normalized across individuals to the first measurement and all time points in the study are used (HbA1C $n=94$, samples = 836; FPG $n=94$, samples = 843; hsCRP $n=92$, samples 777). Each analyte was modeled separately and the two-sided *t*-test was used to determine the *P* value for each analyte effect. A multiple testing correction was performed and molecules were considered significant when Benjamini–Hochberg FDR < 0.2. Model estimates were normalized in each condition so the maximum value equal 1 and the minimal value equal −1. **e**, Integrative pathway analysis using IMPaLa[67] of proteins and metabolites associated with HbA1C ($n=94$, samples = 836), FPG ($n=94$, samples = 843) and hsCRP ($n=92$, samples 777) as determined by the dynamic models (Benjamini–Hochberg FDR < 0.2 at molecule level). Significance of pathways was determined by the hypergeometric test (one-sided) followed by Fisher's combined probability test (one-sided) to determine combined pathway significance (Benjamini–Hochberg FDR < 0.05). The *n*'s of proteins and metabolites for each pathway are provided in Supplementary Tables 15, 17 and 19. **f**, Molecules selected in SSPG and OGTT prediction models and associated coefficients. For SSPG prediction, lipidomics data were used in addition to the multi-omics measures. MSE, mean square error.

unsaturated fatty acid (FDR = 8.2×10^{-4}) and glycerophospholipid metabolism (FDR = 2.88×10^{-3}), FPG associated with amino acid (FDR = 7.4×10^{-4}) and bile acid metabolism (FDR = 4.6×10^{-3}).

The dynamic model analysis revealed more commonalities between changes in glucose measures and inflammation (Fig. 3d,e, Extended Data Fig. 5 and Supplementary Tables 14–19). As expected, hsCRP positively associated with inflammatory proteins including MIG (FDR = 1.4×10^{-4}) and IP10 (FDR = 3.9×10^{-22}) as well as immune pathways including 'complement activation' (FDR = 8.7×10^{-16}), 'innate immune system' (FDR = 8.3×10^{-14}) and 'oxidative damage' (FDR = 3.0×10^{-6}). Both HbA1C and hsCRP positively associated with total white blood cells, monocytes and neutrophils consistent with previous findings[23]. In addition, hepatocyte growth factor (HGF) associated with HbA1C and hsCRP, consistent with its role in glucose metabolism and modulation of inflammatory response[24]. We also observed that FPG and HbA1C both associated with 'leukotriene biosynthesis' that contributes to inflammation and leads to insulin resistance[25]. HbA1C also associated with additional pathways related to lipid metabolism including 'plasma lipoprotein assembly' and 'chylomicron assembly', thus further demonstrating the connections among inflammation, lipid metabolism and metabolic regulation of glucose.

Multi-omics prediction of SSPG and OGTT. The modified insulin suppression test is a clinically important direct measure of peripheral insulin resistance but is expensive and labor-intensive, and requires 6 h. The 2-h OGTT is a sensitive test for diabetes and is less expensive, but still inconvenient. Thus, we evaluated how well multi-omics measurements could predict the results of these tests. Using a Bayesian network algorithm, we first identified highly predictive features followed by ridge regression modeling using these features[26,27]. The SSPG prediction model using all omes achieved a cross-validated R^2 of 0.87 (final model MSE = 0.16) compared to an R^2 of 0.59 (MSE = 0.55) using only clinical data (Fig. 3f and Supplementary Table 20). We also compared predictive models using clinical data plus each single ome and found that the transcriptome (R^2 = 0.88, MSE = 0.15), metabolome (R^2 = 0.80, MSE = 0.31) and microbiome models (R^2 = 0.78, MSE = 0.26) had the best predictive accuracy for SSPG. Similarly, the multi-omic prediction model for OGTT (R^2 = 0.71, MSE = 0.24) was superior to the clinical data only model (R^2 = 0.42, MSE = 0.71) (Fig. 3f and Supplementary Table 21). The transcriptome had the best predictive accuracy of the single ome models (R^2 = 0.62, MSE = 0.30). Molecules that were found to be consistent across multiple SSPG models included the TGL/HDL (high-density lipoprotein) ratio, the protein IL-1RAP; the lipid hexosylceramide (HCER)(24:0), the MAP3K19 transcript and a Ruminococcaceae family microbe. The relationship between insulin resistance and TGL/HDL ratio has already been described[28] and other measures are emerging[29–31]. There was little overlap between SSPG and OGTT predictors, thus supporting the idea that these measures reflect different underlying biology. The increased predictive performance with multi-omics measurements compared to clinical laboratory results alone illustrates the benefit of multi-omics data.

Other metabolic disorders. Other clinical abnormalities were observed in sodium, potassium and liver enzymes (ALT) as well as microalbuminuria and macroalbuminuria (Supplementary Table 2). People with pre-DM and DM are at higher risk for liver steatosis and albuminuria. Using the American Gastroenterological Association (AGA) Guidelines[32] for health normal references (males: 25–33 $IU\,l^{-1}$; females: 19–25 $IU\,l^{-1}$) revealed that the majority of participants (83%) had at least one elevated healthy visit ALT and 41% had elevations at all healthy time points. Given the AGA recommendations for ultrasound screening[32], our findings suggest that screening for nonalcoholic fatty liver disease is indicated in the majority of our population.

One participant had substantially more outlier RNA molecules (ninety-fifth percentile) than the rest of the cohort. These outliers were related to toxicity pathways including oxidative stress and hepatic abnormality pathways (Extended Data Fig. 6a and ref. [10]). The participant had mild elevation in ALT accompanied by increases in bile acids and glutamyl dipeptides (Extended Data Fig. 6b), and was later diagnosed with mild hepatic steatosis. However, many participants had mild ALT elevations and at least five had hepatic steatosis; thus, these clinical findings are not sufficient to explain the RNA-seq outlier status. Although multiple omics and other measures point to aberrant hepatic function, clinical manifestations were unclear and this individual will be tracked for hepatic abnormalities.

Cardiovascular health profiling. Atherosclerotic cardiovascular disease (ASCVD) is a major cause of mortality and morbidity associated with insulin resistance and DM[33]. We assessed the American Heart Association ASCVD risk score, estimating 10-year risk of heart disease or stroke on all participants[34] at study entry. We also followed longitudinal trajectories of dyslipidemia and systemic hypertension. Enhanced cardiovascular profiling was performed on 43 participants and included (1) vascular ultrasound and echocardiography to assess for subclinical atherosclerosis, arterial stiffness or early stage adverse ventricular remodeling or dysfunction and (2) emerging biomarkers assessment to interrogate oxidative stress, inflammation, immune regulation, myocardial injury and myocardial stress pathways[35–37].

Cardiovascular risk profiles. At study entry, 24 patients (22.6%) had an ASCVD risk score ≥7.5%, a threshold often used to guide primary prevention[34] (Fig. 4a). Total cholesterol and blood pressure measurements indicate that self-report underestimated the prevalence of dyslipidemia (Fig. 4b) and 18 participants learned they had stage II hypertension during the study.

Clinical discoveries through enhanced clinical phenotyping. Wearable and cardiovascular imaging led to important clinical discoveries. Wearable heart rate monitoring identified two participants with nocturnal supraventricular tachycardia, leading to the diagnosis of obstructive sleep apnea in one and atrial fibrillation secondary to sleep apnea in the other. In the subgroup of participants who had enhanced cardiovascular imaging studies, we discovered two major health findings: one cardiac finding associated with a pathogenic mutation in the *RPM20* gene, and one non-cardiac finding (Supplementary Table 2). Fitness assessment using percentage predicted oxygen consumption (maximal oxygen consumption relative to a healthy person of the same age and weight) identified three participants with values below 70% suggestive of a reduction in exercise capacity that has been associated with poorer health outcomes[38] (Extended Data Fig. 7a). Subclinical atherosclerosis was found in six participants leading to a recommendation to increase statin dose (Extended Data Fig. 7b). Overall, there were 15 important clinical findings through these enhanced tests (Supplementary Table 2).

Cardiovascular events, pharmacogenomic and transcriptomic findings. Five participants had cardiovascular events during the course of the study including stroke (n = 3), unstable angina (n = 1) and stress-induced cardiomyopathy (n = 1). All had elevated hsCRP levels before their event. Two participants with incident strokes had pharmacogenomic variants that could partially explain suboptimal response to the chosen therapy. One participant on aspirin for stroke prevention had a catechol-*O*-methyltransferase Val/Val genotype (rs4680), which has a 85% increased risk of cardiovascular events in female aspirin users compared to placebo controls[39]. The other participant with incident stroke was an intermediate clopidogrel metabolizer phenotype (*CYP2C19**2 (rs4244285)/*CYP2C19**17

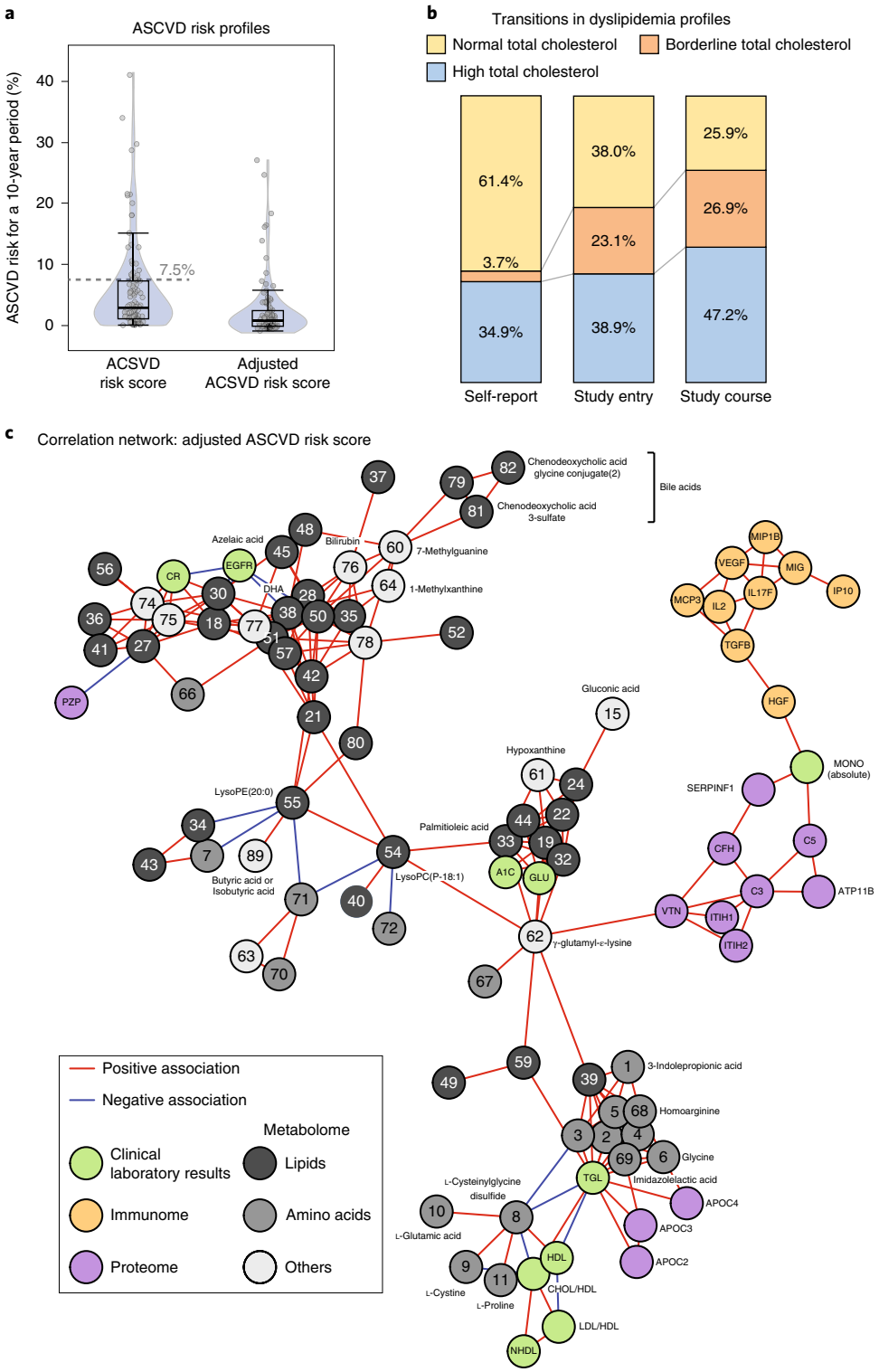

Fig. 4 | Clinical longitudinal cardiovascular health profiling and multi-omics correlation network of adjusted ASCVD risk. a, Distribution of ASCVD risk scores and adjusted ASCVD risk scores ($n=108$). The box plot shows the first (lower edge of box), median (middle line) and third (upper edge of box) quartiles. The upper whisker is the third quartile + 1.5× (interquartile range) and the lower whisker is the lowest data point. **b**, Self-reported cholesterol status versus measured total cholesterol profiles at study entry and over the course of the study ($n=108$). **c**, Multi-omics correlation network of molecules associated with adjusted ASCVD risk score ($n=77$ participants) using Spearman correlation and multiple testing correction of q value < 0.2. Correlations between molecules were then calculated using Spearman correlation and considered significant if Bonferroni-corrected $P<0.1$. Only molecules belonging to the main network were plotted.

(rs12248650)) and had a second stroke while on clopidogrel. Intermediate metabolizers of clopidogrel were common in our study (31/88 (35%)) and 4/88 (4.5%) were poor metabolizers. Additional pharmacogenomic variants related to the common cardiovascular medications of statins and coumadin were found in 26 and 30 participants, respectively (Supplementary Table 22).

We also analyzed 14 of 32 genes associated with stroke and stroke types[40] that were robustly detected in our RNA-seq dataset. Outlier analysis revealed that two of the five participants with cardiovascular events had the highest composite Z scores at clinically relevant time points including post-stent placement (Z score = 33.2, FDR = 6.9×10^{-6}), mid-infection ($Z = 40.4$, FDR = 3.2×10^{-9}) for one participant and transition to diabetes ($Z = 30.1$ and 24.1) for the other (Extended Data Fig. 7d,e). Thus, expression levels of genes related to stroke were outliers and associated with significant health issues.

Multi-omics analysis of ASCVD risk. We calculated pair-wise associations by using Spearman correlation between multi-omics measures and adjusted ASCVD risk score and constructed a correlation network (Fig. 4c and Supplementary Tables 23 and 24). This analysis revealed relationships between clinical and omics measures such as monocytes bridging cytokines and complement proteins, and triglyceride and cholesterol measures linking to apolipoproteins. Among immune proteins, the interferon-gamma pathway (MIG, IP10), interleukin (IL)-2, vascular endothelial growth factor alpha and HGF) were strongly associated with the ASCVD risk score. The interferon-gamma pathway has been recently found to play a key role in atherosclerosis on the basis of population-based studies[41–45]. IL-2 has been shown to be associated with atherosclerosis through its role in T-cell mediated inflammation[45]. HGF is involved in the survival of endothelial cells and is emerging as a risk factor of outcome[42,43]. Our network also highlighted several molecules that are emerging in cardiovascular disease research including complement and free fatty acids as well as γ-glutamyl-ε-lysine (reported in diabetic nephropathy), hypoxanthine, methylxanthine (associated with coffee consumption) and bile acids[46–48].

In participants who underwent cardiovascular imaging, we also performed a correlation network analysis that shows how ASCVD risk, enhanced imaging and selected circulating protein markers associate together (Extended Data Fig. 7c and Supplementary Table 0). ASCVD score was closely related to HGF, which itself was closely related to inflammatory cytokines IL-1B and IL-18, part of the inflammasome complex. Exercise capacity as assessed with peak VO_2 was closely associated with GDF-15, a transforming growth factor that is associated with cardiovascular mortality risk[49] and leptin, a hormone that regulates appetite[50]. These findings demonstrate an interaction between inflammation and ASCVD risk and suggest new opportunities for personalized risk stratification, beyond those currently available.

Oncological, hematological and immune profiling. Exome sequencing also led to several important oncological, hematological and immune-related clinical discoveries. Eight participants learned they had clinically actionable genetic variants associated with increased oncologic risk, such as *APC*, *SDHB*, *BRCA1*, *MUTYH*, *CHEK2*, and hematologic risk (*PROS1*) (Supplementary Table 2). In one case, follow-up screening led to discovery of an early stage papillary thyroid cancer, and the participant was able to elect thyroid preserving surgery due to early detection.

B-cell lymphoma discovery and longitudinal outlier analysis. Abdominal ultrasound imaging revealed splenomegaly and large para-aortic lymph nodes in one participant (Fig. 5a); immediate clinical work-up (Fig. 5b,c and Supplementary Table 2) led to diagnosis of B-cell lymphoma. Longitudinal omics outlier analysis revealed a striking increase (greater than five-fold) in the cytokine MIG that started over a year before diagnosis and returned to baseline after treatment (Fig. 5d). Its early elevation suggests possible use as an early biomarker, consistent with other studies[51–53]. Although it is probably important in a number of cancers[54], our data demonstrate MIG's use as a longitudinal marker of disease. A notable decrease in histidine-rich glycoprotein was also evident at diagnosis (Supplementary Table 25), consistent with its previously reported role in inhibiting tumor growth and metastasis[55,56].

The functional association network using proteins that were in the ninety-fifth percentile at the time of diagnosis relative to all the healthy visits in the study illustrates the central role of MIG in orchestrating other cytokines, namely ENA78, IL17A and VCAM1 (Fig. 5e). Pathways involved in inflammation/immune response as well as cell proliferation and migration were enriched at time of diagnosis (Supplementary Table 26). The participant's gut microbiome Shannon diversity also changed with time ($P = 0.0041$), primarily declining in the 2 years before diagnosis, with a nadir at diagnosis (Fig. 5f) and increasing with treatment. Outlier microbes (ninety-fifth percentile) at time of diagnosis included low proportions of the genera Clostridium IV, Lachnospiraceae incertae sedis, unclassified Clostridiales and Ruminococcaceae and elevated proportions of the class Gammaproteobacteria (Supplementary Table 25). Similar to our findings in participants with low diversity before DM diagnosis, at the point of lowest diversity, the phylum Bacteroides predominated (84%). Altogether, we demonstrate that longitudinal molecular outlier analysis can identify deviations in key molecules associated with disease to reveal potential biomarkers and give insights into underlying biological mechanisms associated with the disease.

Hematologic, immune and infection profiling. Comprehensive clinical laboratory results identified many important health-related findings. Thirty participants had hemoglobin or hematocrit in the anemic range, including 28 participants without previously known anemia (hemoglobin: males <135 mg ml^{-1}, females <117 mg ml^{-1}). In participants with anemia, mean corpuscular volume was low (<82 femtoliters) in 26.7% ($n = 8$) suggesting microcytic anemia, 10% ($n = 3$) had an elevated mean corpuscular volume (>98 femtoliters) with normal mean corpuscular hemoglobin concentration and the remainder had normocytic anemia. One of these participants was discovered to have the alpha thalassemia trait after referral to their physician for anemia evaluation.

Immunological profiling with IgM identified one participant with a significantly elevated IgM (Fig. 5g), which led to a clinical diagnosis of MGUS. Nine participants were noted to have persistently low IgM (two or more IgM < 0.3 mg ml^{-1}). Four participants had subsequent clinical evaluation of IgA and IgG that led to identification of IgG monoclonal gammopathy and subsequent diagnosis of smoldering myeloma in one participant. The discovery of MGUS and smoldering myeloma precancers has important implications in elevated risk and screening for cancer[57,58].

During the study, wearable monitoring detected temperature and heart rate abnormalities related to inflammatory disturbances as measured by hsCRP ($n = 4$). In one of the participants, these findings resulted in diagnosis of Lyme disease[2]. Thus, important health information related to hematologic, immune and infection systems were revealed by a variety of different approaches.

Effect of iPOP participation on participants. The deep phenotyping profiling had an effect on the majority of the participants by (1) encouraging appropriate risk-based screening including genetic counseling, (2) facilitating clinically meaningful diagnosis, (3) potentially informing therapeutic choices (mechanistic or pharmacogenomic information) and (4) increasing awareness leading to diet and physical activity modifications. Overall, we found over 67 major clinically actionable health discoveries spanning various area including metabolic, cardiovascular, heme/oncological and infectious using standard clinical, enhanced and emerging technologies (Fig. 6a and Supplementary Table 2).

Fifty-eight participants were surveyed mid-to-late-study about the effect of participating in the study including changes on food

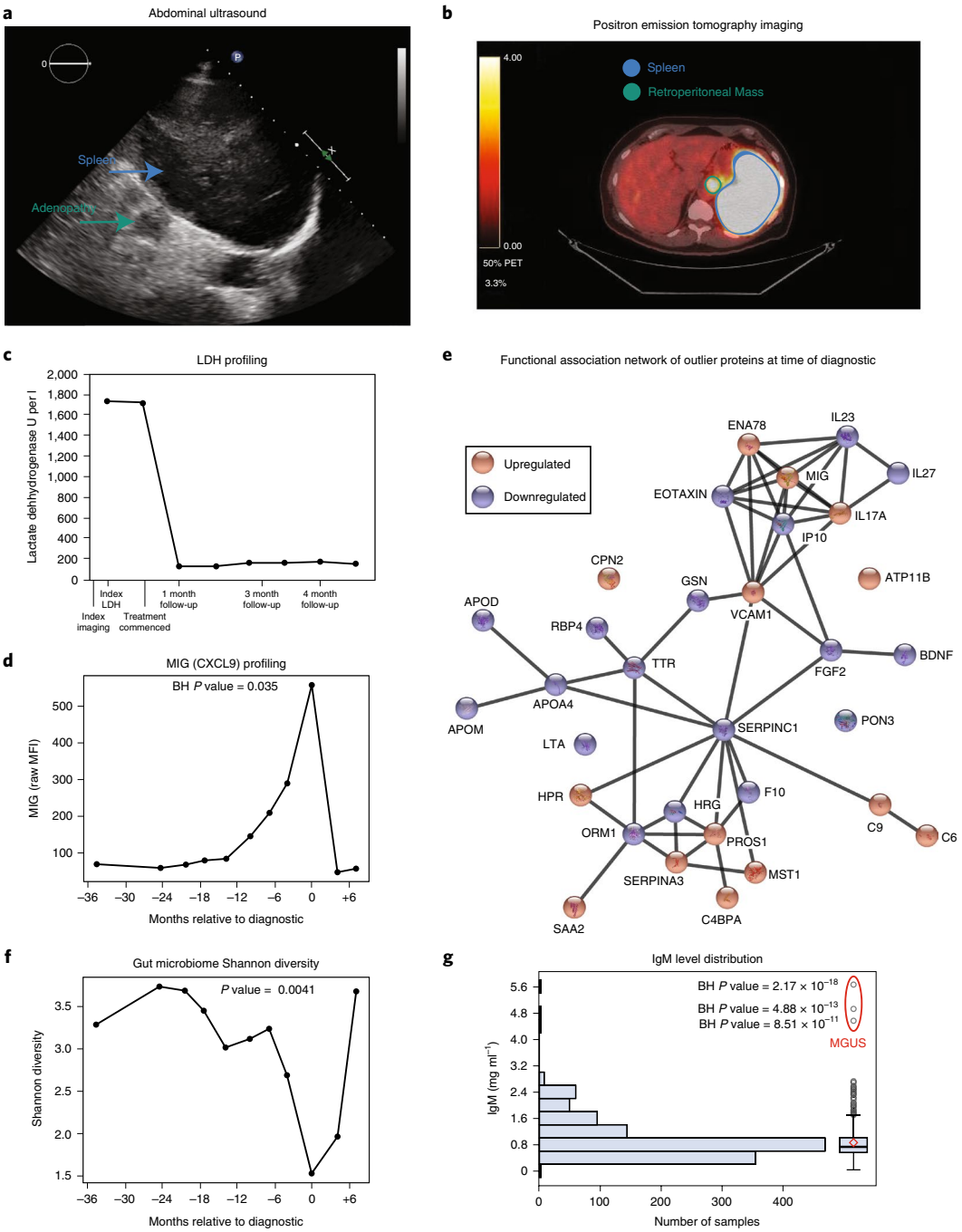

Fig. 5 | Oncologic discoveries. a, Abdominal ultrasound image where a mildly enlarged spleen measuring approximately 13 cm in craniocaudal dimension can be seen. **b**, Positron emission tomography (PET) imaging where a large retroperitoneal mass with high fluorodeoxyglucose and intensely focal hypermetabolism occupying the majority of the spleen can be seen. **c**, Lactate dehydrogenase (LDH) levels at time of index imaging and after starting chemotherapy. **d**, Levels of MIG (CXCL9) demonstrating an increase starting a year before diagnosis that peaks at time of diagnosis and goes back to baseline after treatment ($n = 11$ samples). Benjamini–Hochberg (BH) P value (two-sided) was calculated on MIG Z scores assuming a normal distribution across all healthy visits in the cohort ($n = 601$ samples). **e**, Functional association network of outlier proteins (ninety-fifth percentile) at time of diagnostic. This analysis was performed using the web tool STRING[68] (https://version-10-5.string-db.org/). Edges correspond to known, predicted or other interactions. **f**, Shannon diversity of the gut microbiome decreasing months before diagnosis, reaching a minimum value at time of diagnostic and returning to baseline after treatment ($n = 11$ samples). Trajectory was then modeled using a general additive model that separates the linear ($\beta = -0.197$, $P = 0.002$ (two-sided t-test)) and non-linear (d.f. = 3, $P = 0.0112$ (one-sided chi square)) components. An F-test (one-sided) was used to compare the model including time to the null model. **g**, IgM (immunoglobulin M) level distribution in the cohort ($n = 109$, samples 1,111). Benjamini–Hochberg P value (two-sided) was calculated on IgM Z scores assuming a normal distribution across all visits in the cohort. Outlier visits are from a participant that was diagnosed with monoclonal gammopathy of undetermined significance (MGUS). The box plot shows the first (lower edge of box), median (middle line) and third (upper edge of box) quartiles. The upper whisker is the third quartile + 1.5× (interquartile range) and the lower whisker is the lowest data point. The diamond is the mean.

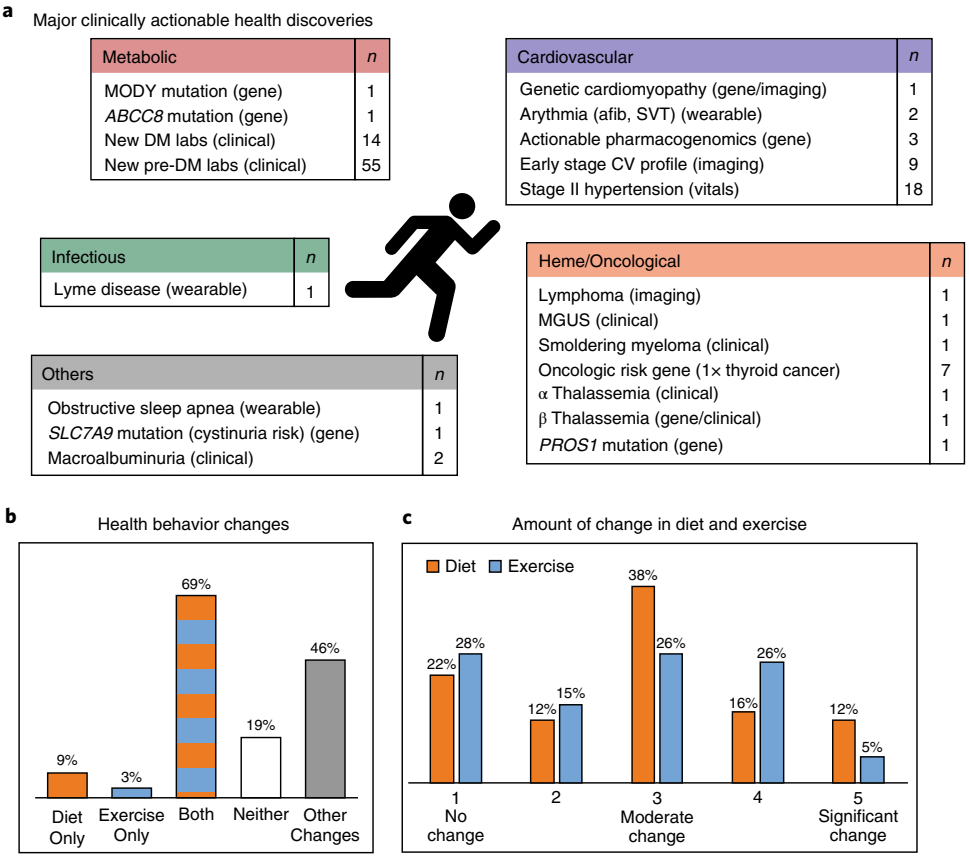

Fig. 6 | Summary of major clinically actionable health discoveries and participant health behavior change. a, Summary of clinically relevant health discoveries: 67 discoveries were considered major and the 55 pre-DM results were not included in this count. **b**, Diet and physical activity modifications. **c**, Amount of change made in diet and exercise (five-point scale was used with 1 being no change and 5 being a significant change). afib, atrial fibrillation; SVT, supraventricular tachycardia; CV, cardiovascular; MODY, maturity onset diabetes of the young; MGUS, monoclonal gammopathy of undetermined significance.

and exercise habits, health findings and their sharing of results with their personal doctors, family and others. Eighty-one percent reported some change in diet and/or exercise habits (Fig. 6b). In addition, almost half reported changing other health behaviors as a result of the study, including improving sleep, reducing stress, adding fiber and supplements to their diet, more careful self-examinations, recording food intake, attending a fitness camp and general lifestyle changes (Supplementary Table 27). Figure 6c shows the amount of change in diet and exercise. Participants also reported that their wearable device kept them accountable for exercising and more mindful to take walking breaks. Others reported using wearables to monitor sleep.

The majority of participants had discussed study results with their family (71%) and physicians (68%). Physician discussions led to follow-up testing in 29% of the cases. Additional testing included having children tested for gene mutation, colonoscopy, additional eye exams, cardiac calcium scan, positron emission tomography scan to evaluate lymphoma, repeating study tests (echocardiogram, pulmonary function tests) in the clinical setting, extra screening for macular degeneration risk and additional tests for diabetes-related studies (SSPG and the Quantitative Sudomotor Axon Reflex Test). Participants were also asked about the effect of SSPG testing and CGM monitoring (Supplementary Table 28). Eight participants who used a CGM monitor reported that it helped them make different dietary and meal frequency choices to reduce their blood sugar spikes. SSPG results motivated at least two participants to change their activity and diet and were reassuring to others. Therefore, overall, a myriad of positive behavior modifications and follow-up tests resulted from study participation.

Discussion

Our study found that combining untargeted multi-omics and physiological longitudinal profiling with targeted profiling of metabolic and cardiovascular risk led to actionable health discoveries and meaningful physiological insights building on our previous work[3]. Our targeted profiling approach enabled us to connect longitudinal profiling of glucose metabolism with multi-omics profiling facilitating the precision medicine goal of defining diseases on the basis of molecular mechanisms and pathophysiology[1]. The untargeted longitudinal big data approach led to a number of discoveries in other areas such as cardiology, oncology, hematology and infectious disease, indicating that broad profiling is valuable for disease detection in many different areas. We capitalized on the depth of longitudinal profiling to identify deregulated molecules and pathways associated with the transition from health to disease.

The study informed more than half the participants of their pre-DM and DM status, dyslipidemia and hypertension, which led many to institute diet and physical activity lifestyle changes. Our enhanced clinical assays including OGTT, beta-cell function assessment, insulin resistance and CGM in combination with standard clinical tests (FPG and HbA1C) improved characterization of pre-DM and DM status. The in-depth physiological profiling identified individual mechanisms of glucose dysregulation that has important implications for implementation of personalized treatments. Our

findings are consistent with a recent study that found that treatments based on the current classification are not well tailored to mechanistic subtypes[59] and proposed five subtypes of adult onset DM. Deeper molecular understanding of progression to DM and its characteristics in the individual may help tailor therapy to its underlying pathophysiology and will probably identify additional subtypes and also inform stratification of CVD risk[60]. The superiority of using multi-omics data for SSPG prediction compared to standard measures illustrates the value of multi-omics data to help provide a molecular taxonomy of disease[1], as well as replace expensive burdensome tests for insulin resistance with a simple blood test. Microbiome measures were also a good predictor of SSPG when combined with clinical measures and SSPG inversely correlated with Shannon diversity further demonstrating the intricate relationship between gut microbes and insulin resistance consistent with our multi-omics study of weight gain[61].

Although the majority of our exome sequencing findings were in the oncologic realm, several important metabolic exome findings were found including a MODY mutation with implications for medication management, a *RBM20* mutation related to dilated cardiomyopathy and numerous pharmacogenomic variants that have important health implications[62]. Furthermore, two participants experienced vascular events, unaware of relevant pharmacogenomics information that could have suggested alternative treatments. Thus, we expect complex genetic risk assessment such as the information learned in this study to be incorporated into risk management and tailored treatment of disease[63].

Imaging plays a central role in precision health initiatives, enabling the early detection of oncological and systemic disease[64]. In our study, imaging helped detect dilated cardiomyopathy (in the patient with *RBM20* mutation), early stage atherosclerotic disease and a case of asymptomatic lymphoma. Wearable sensors are emerging as a transformative technology for precision health and medicine and heart rate monitoring led to the diagnosis of atrial fibrillation, sleep apnea and detection of Lyme disease in participants. Large population-based initiatives such as 'myHeart counts' are evaluating the potential of wearable heart sensors to detect subclinical atrial fibrillation[7] and electrocardiographic monitoring is now available in consumer wearable devices[65]. Our findings also suggest a role for CGM in diabetes prevention by identifying unrecognized glucose dysregulation[6], and enabling the individual to optimize their diet on the basis of personalized glycemic responses.

Our multi-omics analysis also provided important insights into ASCVD risk, highlighting the importance of systemic inflammation. Although our study was not powered for outcome analysis, all five participants with incident cardiovascular events had subclinical inflammation. Furthermore, correlation network analysis highlighted the role of monocytes, HGF, IL-2, MCP-3 and interferon-gamma cytokines including MIG and IP10 and other molecules in cardiovascular health. These analytes are involved in inflammation and are emerging in the context of ASCVD[41–43,45,66].

Untargeted longitudinal outlier analysis of the period leading up to the diagnosis of lymphoma illustrates the importance of longitudinal multi-omics analysis for biomarker and pathway discoveries. We identified potential critical biomarkers (for example, MIG) and changes in the microbiome up to 1 year before diagnosis demonstrating the power of monitoring molecules longitudinally to detect deviations from the healthy baseline. Outlier biomarkers at time of diagnosis illustrated deregulated pathways related to inflammation, cell proliferation and cell migration that shed light on underlying dysregulated biological mechanisms associated with the disease. Further work will be needed to streamline the investigation of untargeted discoveries in precision medicine research. Given the need for early biomarkers for cancer detection, longitudinal multi-omics analyses represent an important tool for meeting this need. In addition to individual molecule monitoring, omics profiles provide the opportunity to detect outliers relative to a matched-healthy population. Clinical outlier analysis identified one participant with MGUS where early diagnosis with follow-up can increase survival time in individuals who progress to an associated malignancy[57]. While some omics outlier profiles could be clearly connected to an underlying health condition, the case of the participant with significant RNA-seq outliers illustrates the challenges of interpreting the clinical relevance of outlier analysis results with emerging measures. While precision medicine approaches have the potential for unnecessary anxiety and overtesting, we did not observe this in our population.

In the rapidly evolving field of precision medicine, this study should be assessed in the context of methodological considerations. Our cohort comprised highly educated volunteers, and therefore probably had a self-selection bias. Although this may affect the generalizability of our findings for behavioral changes, it is less likely to affect the underlying biological associations of multi-omics with glucose measures. A study strength is its ethnic diversity, which is greater than that in other longitudinal multi-omics studies[4,5]. In sum, we demonstrate the feasibility of a longitudinal precision health and medicine approach that builds on sound molecular and physiological phenotyping. We show that in-depth physiological and multi-omics characterizations are likely to further refine risk stratification. The intensive longitudinal study design demonstrates how a small longitudinal cohort can yield important health and discovery findings. In the future, it will be possible to design personalized testing programs on the basis of individual disease risk and longitudinal marker trajectories as well as evaluate the cost-value of these approaches for individuals and health care systems.

Online content

Any methods, additional references, Nature Research reporting summaries, source data, statements of data availability and associated accession codes are available at https://doi.org/10.1038/s41591-019-0414-6.

Received: 10 May 2018; Accepted: 6 March 2019;
Published online: 8 May 2019

References

1. National Research Council (US) Committee on a framework for developing a new taxonomy of disease. *Toward Precision Medicine: Building a Knowledge Network for Biomedical Research and a New Taxonomy of Disease* (National Academies Press, 2012).
2. Li, X. et al. Digital health: tracking physiomes and activity using wearable biosensors reveals useful health-related information. *PLoS Biol.* **15**, e2001402 (2017).
3. Chen, R. et al. Personal omics profiling reveals dynamic molecular and medical phenotypes. *Cell* **148**, 1293–1307 (2012).
4. Price, N. D. et al. A wellness study of 108 individuals using personal, dense, dynamic data clouds. *Nat. Biotechnol.* **35**, 747–756 (2017).
5. Perkins, B. A. et al. Precision medicine screening using whole-genome sequencing and advanced imaging to identify disease risk in adults. *Proc. Natl Acad. Sci. USA* **115**, 3686–3691 (2018).
6. Hall, H. et al. Glucotypes reveal new patterns of glucose dysregulation. *PLoS Biol.* **16**, e2005143 (2018).
7. McConnell, M. V. et al. Feasibility of obtaining measures of lifestyle from a smartphone app: the myheart counts cardiovascular health study. *JAMA Cardiol* **2**, 67–76 (2017).
8. Dinneen, S., Gerich, J. & Rizza, R. Carbohydrate metabolism in non-insulin-dependent diabetes mellitus. *N. Engl. J. Med.* **327**, 707–713 (1992).
9. Varghese, R. T. et al. Mechanisms underlying the pathogenesis of isolated impaired glucose tolerance in humans. *J. Clin. Endocrinol. Metab.* **101**, 4816–4824 (2016).
10. Zhou, W. et al. Complex host-microbial dynamics in prediabetes revealed through longitudinal multi-omics profiling. *Nature* (in the press).
11. 1000 Genomes Project Consortium. et al. A global reference for human genetic variation. *Nature* **526**, 68–74 (2015).
12. Rego, S. et al. High frequency actionable pathogenic exome variants in an average-risk cohort. *Cold Spring Harb. Mol. Case Stud.* **4**, a003178 (2018).
13. Pearson, E. R. et al. Genetic cause of hyperglycaemia and response to treatment in diabetes. *Lancet* **362**, 1275–1281 (2003).

14. Cersosimo, E., Solis-Herrera, C., Trautmann, M. E., Malloy, J. & Triplitt, C. L. Assessment of pancreatic β-cell function: review of methods and clinical applications. *Curr. Diabetes Rev.* **10**, 2–42 (2014).
15. Van Cauter, E., Mestrez, F., Sturis, J. & Polonsky, K. S. Estimation of insulin secretion rates from C-peptide levels. Comparison of individual and standard kinetic parameters for C-peptide clearance.*Diabetes* **41**, 368–377 (1992).
16. Matsuda, M. & DeFronzo, R. A. Insulin sensitivity indices obtained from oral glucose tolerance testing: comparison with the euglycemic insulin clamp. *Diabetes Care* **22**, 1462–1470 (1999).
17. Godsland, I. F., Jeffs, J. A. R. & Johnston, D. G. Loss of beta cell function as fasting glucose increases in the non-diabetic range. *Diabetologia* **47**, 1157–1166 (2004).
18. Kanat, M. et al. The relationship between {beta}-cell function and glycated hemoglobin: results from the veterans administration genetic epidemiology study. *Diabetes Care* **34**, 1006–1010 (2011).
19. Iikuni, N., Lam, Q. L. K., Lu, L., Matarese, G. & La Cava, A. Leptin and inflammation. *Curr. Immunol. Rev.* **4**, 70–79 (2008).
20. Hamilton, J. A. GM-CSF in inflammation and autoimmunity. *Trends Immunol.* **23**, 403–408 (2002).
21. Reidy, S. P. & Weber, J. Leptin: an essential regulator of lipid metabolism. *Comp. Biochem. Physiol. A* **125**, 285–298 (2000).
22. Guasch-Ferré, M. et al. Metabolomics in prediabetes and diabetes: a systematic review and meta-analysis. *Diabetes Care* **39**, 833–846 (2016).
23. Twig, G. et al. White blood cells count and incidence of type 2 diabetes in young men. *Diabetes Care* **36**, 276–282 (2013).
24. Oliveira, A. G. et al. The role of hepatocyte growth factor (HGF) in insulin resistance and diabetes. *Front. Endocrinol.* **9**, 503 (2018).
25. Mothe-Satney, I. et al. Adipocytes secrete leukotrienes: contribution to obesity-associated inflammation and insulin resistance in mice. *Diabetes* **61**, 2311–2319 (2012).
26. Tsamardinos, I., Brown, L. E. & Aliferis, C. F. The max-min hill-climbing Bayesian network structure learning algorithm. *Mach. Learn.* **65**, 31–78 (2006).
27. Lagani, V., Athineou, G., Farcomeni, A., Tsagris, M. & Tsamardinos, I. Feature selection with the R Package MXM: discovering statistically equivalent feature subsets. *J. Stat. Softw.* **80**, 1–25 (2017).
28. McLaughlin, T. et al. Use of metabolic markers to identify overweight individuals who are insulin resistant. *Ann. Intern. Med.* **139**, 802–809 (2003).
29. Nowak, C. et al. Protein biomarkers for insulin resistance and type 2 diabetes risk in two large community cohorts. *Diabetes* **65**, 276–284 (2016).
30. Apostolopoulou, M. et al. Specific hepatic sphingolipids relate to insulin resistance, oxidative stress, and inflammation in nonalcoholic steatohepatitis. *Diabetes Care* **41**, 1235–1243 (2018).
31. Gomez-Arango, L. F. et al. Connections between the gut microbiome and metabolic hormones in early pregnancy in overweight and obese women. *Diabetes* **65**, 2214–2223 (2016).
32. Kwo, P. Y., Cohen, S. M. & Lim, J. K. ACG clinical guideline: evaluation of abnormal liver chemistries. *Am. J. Gastroenterol.* **112**, 18–35 (2017).
33. Hu, F. B. et al. Elevated risk of cardiovascular disease prior to clinical diagnosis of type 2 diabetes. *Diabetes Care* **25**, 1129–1134 (2002).
34. Goff, D. C. Jr et al. 2013 ACC/AHA guideline on the assessment of cardiovascular risk: a report of the American College of Cardiology/American Heart Association Task Force on Practice Guidelines. *Circulation* **129**, S49–S73 (2014).
35. Kuznetsova, T. et al. Additive prognostic value of left ventricular systolic dysfunction in a population-based cohort. *Circ. Cardiovasc. Imag.* **9**, e004661 (2016).
36. Wang, T. J. et al. Carotid intima-media thickness is associated with premature parental coronary heart disease: the Framingham Heart Study. *Circulation* **108**, 572–576 (2003).
37. Mitchell, G. F. et al. Arterial stiffness and cardiovascular events: the Framingham Heart Study. *Circulation* **121**, 505–511 (2010).
38. Moneghetti, K. J. et al. Applying current normative data to prognosis in heart failure: the fitness registry and the importance of exercise national database (FRIEND). *Int. J. Cardiol.* **263**, 75–79 (2018).
39. Hall, K. T. et al. Polymorphisms in catechol-O-methyltransferase modify treatment effects of aspirin on risk of cardiovascular disease. *Arterioscler. Thromb. Vasc. Biol.* **34**, 2160–2167 (2014).
40. Malik, R. et al. Multiancestry genome-wide association study of 520,000 subjects identifies 32 loci associated with stroke and stroke subtypes.*Nat. Genet.* **50**, 524–537 (2018).
41. Cross, D. S. et al. Coronary risk assessment among intermediate risk patients using a clinical and biomarker based algorithm developed and validated in two population cohorts. *Curr. Med. Res. Opin.* **28**, 1819–1830 (2012).
42. Ma, H., Calderon, T. M., Fallon, J. T. & Berman, J. W. Hepatocyte growth factor is a survival factor for endothelial cells and is expressed in human atherosclerotic plaques. *Atherosclerosis* **164**, 79–87 (2002).
43. Bell, E. J. et al. Hepatocyte growth factor is positively associated with risk of stroke: the MESA (Multi-Ethnic Study of Atherosclerosis). *Stroke* **47**, 2689–2694 (2016).
44. Chen, X. & Devaraj, S. Monocytes from metabolic syndrome subjects exhibit a proinflammatory M1 phenotype. *Metab. Syndr. Relat. Disord.* **12**, 362–366 (2014).
45. Elkind, M. S. et al. Interleukin-2 levels are associated with carotid artery intima-media thickness. *Atherosclerosis* **180**, 181–187 (2005).
46. Porez, G., Prawitt, J., Gross, B. & Staels, B. Bile acid receptors as targets for the treatment of dyslipidemia and cardiovascular disease. *J. Lipid Res.* **53**, 1723–1737 (2012).
47. Berry, C. E. & Hare, J. M. Xanthine oxidoreductase and cardiovascular disease: molecular mechanisms and pathophysiological implications. *J. Physiol.* **555**, 589–606 (2004).
48. Sane, D. C., Kontos, J. L. & Greenberg, C. S. Roles of transglutaminases in cardiac and vascular diseases. *Front. Biosci.* **12**, 2530–2545 (2007).
49. Wollert, K. C., Kempf, T. & Wallentin, L. Growth differentiation factor 15 as a biomarker in cardiovascular disease. *Clin. Chem.* **63**, 140–151 (2017).
50. Klok, M. D., Jakobsdottir, S. & Drent, M. L. The role of leptin and ghrelin in the regulation of food intake and body weight in humans: a review. *Obes. Rev.* **8**, 21–34 (2007).
51. Charbonneau, B. et al. Pretreatment circulating serum cytokines associated with follicular and diffuse large B-cell lymphoma: a clinic-based case-control study. *Cytokine* **60**, 882–889 (2012).
52. Przewoznik, M. et al. Recruitment of natural killer cells in advanced stages of endogenously arising B-cell lymphoma: implications for therapeutic cell transfer. *J. Immunother.* **35**, 217–222 (2012).
53. Haabeth, O. A. W. et al. Inflammation driven by tumour-specific Th1 cells protects against B-cell cancer. *Nat. Commun.* **2**, 240 (2011).
54. Ding, Q. et al. CXCL9: evidence and contradictions for its role in tumor progression. *Cancer Med.* **5**, 3246–3259 (2016).
55. Rolny, C. et al. HRG inhibits tumor growth and metastasis by inducing macrophage polarization and vessel normalization through downregulation of PlGF. *Cancer Cell* **19**, 31–44 (2011).
56. Johnson, L. D. S., Goubran, H. A. & Kotb, R. R. Histidine rich glycoprotein and cancer: a multi-faceted relationship. *Anticancer Res.* **34**, 593–603 (2014).
57. Go, R. S., Gundrum, J. D. & Neuner, J. M. Determining the clinical significance of monoclonal gammopathy of undetermined significance: a SEER-Medicare population analysis. *Clin. Lymphoma Myeloma Leuk.* **15**, 177–186.e4 (2015).
58. Turesson, I. et al. Monoclonal gammopathy of undetermined significance and risk of lymphoid and myeloid malignancies: 728 cases followed up to 30 years in Sweden. *Blood* **123**, 338–345 (2014).
59. Alqvist E. et al. Novel subgroups of adult-onset diabetes and their association with outcomes: a data-driven cluster analysis of six variables. *Lancet Diabetes Endocrinol.* **6**, P361–P369 (2018).
60. Cauwenberghs, N. et al. Relation of insulin resistance to longitudinal changes in left ventricular structure and function in a general population. *J. Am. Heart Assoc.* **7**, e008315 (2018).
61. Piening, B. D. et al. Integrative personal omics profiles during periods of weight gain and loss. *Cell Syst.* **6**, 157–170.e8 (2018).
62. Whirl-Carrillo, M. et al. Pharmacogenomics knowledge for personalized medicine. *Clinical Pharmacol. Ther.* **92**, 414–417 (2012).
63. Li, J. et al. Decoding the genomics of abdominal aortic aneurysm. *Cell* **174**, 1361–1372.e10 (2018).
64. Douglas, P. S. et al. The future of cardiac imaging: report of a think tank convened by the american college of cardiology. *JACC Cardiovasc. Imag.* **9**, 1211–1223 (2016).
65. Buhr, S. Apple's Watch isn't the first with an EKG reader but it will matter to more consumers. *TechCrunch* https://techcrunch.com/2018/09/12/apples-watch-isnt-the-first-with-an-ekg-reader-but-it-will-matter-to-more-consumers/ (2018).
66. Omer, W., Naveed, A. K., Khan, O. J. & Khan, D. A. Role of cytokine gene score in risk prediction of premature coronary artery disease. *Genet. Test. Mol. Biomarkers* **20**, 685–691 (2016).
67. *Integrated Molecular Pathway Level Analysis* (accessed 27 December 2018); http://impala.molgen.mpg.de/
68. Szklarczyk, D. et al. STRINGv10: protein-protein interaction networks, integrated over the tree of life. *Nucleic Acids Res.* **43**, D447–D452 (2015).

Acknowledgements

Our work was supported by grants from the National Institutes of Health (NIH) Human Microbiome Project (HMP) 1U54DE02378901 (G.M.W. and M.P.S.), an NIH grant no. R01 DK110186-03 (T.L.M.), a NIH National Center for Advancing Translational Science Clinical and Translational Science Award (no. UL1TR001085). This work used the Genome Sequencing Service Center by the Stanford Center for Genomics and Personalized Medicine Sequencing Center (supported by NIH grant no. S10OD020141), the Diabetes Genomics Analysis Core and the Clinical and Translational Core of the Stanford Diabetes Research Center (NIH grant no. P30DK116074). S.M.S.-F.R. was supported by a Department of Veteran Affairs Office of Academic Affiliations Advanced Fellowship in Spinal Cord Injury Medicine and a NIH Career Development Award no. K08 ES028825. G.M.S. was supported by NIH grant no. K08 MH103443. D.H.

was supported by a Stanford School of Medicine Dean's Postdoctoral Fellowship and a Stanford Center for Computational, Evolutionary and Human Genomics Fellowship. M.R.S. was supported by grant nos. P300PA_161005 and P2GEP3_151825 from the Swiss National Science Foundation (SNSF). The content is solely the responsibility of the authors and does not necessarily represent the official views of the NIH, the Department of Veteran Affairs, or the SNSF. We thank S. Chen and B. Lee for their work in metabolomics data production. A. Breschi generously shared her code for the ISR calculations. Finally, we thank the iPOP participants who generously gave their time and biological samples.

Author contributions

S.M.S.-F.R., M.P.S., F.H., K.C., K.M., T.M. and W.Z. contributed to the conceptualization. S.M.S.-F.R., K.C., F.H., M.P.S., T.M., K.M., S.M., W.Z. and S.R. contributed to the methodology. K.C. (ASCVD biomarkers), D.H. (Lipidomics), A.B.G. (Microbiome DADA2 processing), T.M., M.A. and W.Z. (OGTT C-peptide and insulin) contributed to omics generation and/or processing. S.M.S.-F.R., K.C., T.M., W.Z., J.D., M.A., J.W.C., E.S. and P.L. contributed to data curation. K.C., S.M.S.-F.R., T.M., K.M., F.H. and M.P.S. contributed to visualization. S.M.S.-F.R., K.C., T.M., S.M., K.M., O.D.-R., S.R., J.C. and C.R. contributed to formal analysis. S.M.S.-F.R., K.C. and M.P.S. contributed to project administration. M.P.S. and F.H. contributed to supervision. S.M.S.-F.R., F.H., K.C., K.M. and M.P.S. contributed to writing and preparing the original draft. S.M.S.-F.R., K.C., K.M., F.H., M.P.S., W.Z., A.B.G., D.H., J.D., G.M.S, T.M., M.T., D.P., T.L.M., A.J.B., M.R.S. and S.A. contributed to review and editing. K.M., F.H. and J.W.C. contributed to cardiovascular clinical data collection and investigation. W.Z., S.R., M.A., P.L., D.P., M.T., T.L.M. and S.M.S.-F.R. contributed to iPOP/iHMP clinical data collection/investigation. W.Z., S.R.L, M.P.S., T.L.M., E.S. and G.M.W. contributed to iPOP/iHMP project administration. K.C. (metabolomics), S.A. (proteomics), M.R.S. (DNA, RNA-seq), W.Z. (microbiome, cytokines, and overall omics data), Y.Z. (microbiome), T.M. and D.H. (batch correction methodology for proteomics) contributed to iPOP/iHMP omics raw data processing. M.P.S., G.M.W., T.L.M. and E.S. contributed to iPOP/iHMP funding acquisition.

Competing interests

M.P.S. is a cofounder of Personalis, SensOmics, January, Filtricine, Qbio and Akna and an inventor on provisional patent number 62/814,746 'Methods for evaluation and treatment of glycemic dysregulation and applications thereof'. S.M.S.-F.R., K.C., W.Z., T.M. and S.M. are also listed as inventors. A.J.B. reports grants and non-financial support from Progenity, grants and personal fees from NIH (multiple institutes) and Genentech, and grants from L'Oreal, personal fees from NuMedii, Personalis, Lilly, Assay Depot, Geisinger Health, GNS Healthcare, uBiome, Roche, Wilson Sonsini Goodrich & Rosati, Orrick, Herrington & Sutcliffe, Verinata, 10x Genomics, Pathway Genomics, Guardant Health, Gerson Lehrman Group, Nuna Health, Samsung, Capital Royalty Group, Optum Labs, Pfizer, AbbVie, Bayer, Three Lakes Partners, HudsonAlpha, Tensegrity, Westat, FH Foundation, WuXi, FlareCapital, Helix, Roam Insights, Autodesk, Regenstrief Institute, American Medical Association, Precision Medicine World Conference, and Mars during the conduct of the study. A.J.B. has pending patent Atul J. Butte, Keiichi Kodama, Methods for diagnosis and treatment of non-insulin dependent diabetes mellitus, published August 4, 2011, WO2011094731 and US20130071408; patent Joel T. Dudley, Atul J. Butte, Method and System for Computing and Integrating Genetic and Environmental Health Risks for a Personal Genome, published April 26, 2012, US20120101736 with royalties paid to Personalis; patent Joel T. Dudley, Atul J. Butte, Method And System For Functional Evolutionary Assessment Of Genetic Variants, published April 11, 2013, US20130090909 with royalties paid to Personalis; patent Konrad Karczewski, Michael Snyder, Atul J. Butte, Joel T. Dudley, Eurie Hong, Alan Boyle, J. Michael Cherry, Method and System for Assessment of Regulatory Variants in a Genome, published May 9, 2013, US20130116931 with royalties paid to Personalis; and patent Frederick Dewey, Euan Ashley, Carlos Daniel Bustamante, Atul Butte, Jake Byrnes, Rong Chen, Phased Whole Genome Genetic Risk In A Family Quartet, published March 28, 2013, US20130080068, with royalties paid to Personalis; Stanford University pays royalties each year on licensed intellectual property.

Additional information

Extended data is available for this paper at https://doi.org/10.1038/s41591-019-0414-6.

Supplementary information is available for this paper at https://doi.org/10.1038/s41591-019-0414-6.

Reprints and permissions information is available at www.nature.com/reprints.

Correspondence and requests for materials should be addressed to F.H. or M.P.S.

Methods

Participant consent and accrual. Participants were recruited from the Stanford University surrounding community with the goal of enriching the cohort with individuals at risk for type 2 diabetes and thus included individuals who expressed interest in other studies related to diabetes. Participants were enrolled as part of Stanford's iPOP research study (IRB 23602), which entails longitudinal multi-omics profiling of a cohort of adult volunteers enriched for prediabetes. There was no payment required to participate in the study and participants were not paid for their time. This study is part of the NIH integrated Human Microbiome Project (iHMP).

Design, setting and participants. The iPOP study is a longitudinal prospective cohort study[69] containing 109 individuals (Extended Data Fig. 1a). Inclusion criteria were ages 25–75, body mass index (BMI) between 25 and 40 $kg\,m^{-2}$ and 2-h OGTT in the normal or prediabetic range (<2.0 $mg\,ml^{-1}$). Exclusions included active eating disorder, hypertriglyceridemia >4.0 $mg\,ml^{-1}$, uncontrolled hypertension, heavy alcohol use, pregnancy/lactation, previous bariatric surgery and active psychiatric disease. After meeting initial recruitment goals, we expanded our inclusion criteria to include people with diabetes and people with normal BMI into the study. Participant demographics are summarized in Supplementary Table 1 with detailed data provided in Supplementary Data Tables 1–3. Of note, our cohort is slightly different from that in the main iHMP paper[10]. We excluded one participant who had no clinical history or follow-up information available and included four participants with clinical discoveries who entered the study after 2016 and thus had no omics data available.

The cohort was recruited over a number of years, with the first participant starting in 2010. The study design has been described in detail previously[69]. Briefly, participants were asked to donate samples (that is, fasted blood and stool) quarterly when healthy and more frequently when sick (viral infection), after immunization and various other events such as after taking antibiotics and going through colonoscopy. Samples collected throughout December 2016 were used for multi-omics analysis and corresponds to a median participation duration of 2.8 years. Standard and enhanced clinical laboratory data and participant surveys were available throughout June 2018. Most analyses were performed using only healthy time points. The text indicates whether all time points were used.

Measurements. All blood samples were collected after an overnight fast and were used to perform standard and enhanced clinical tests as well as emerging assays (Fig. 1). Standard tests included: FPG, HbA1C, fasted insulin, basic lipid panel, complete metabolic panel, CBC with differential and others (Supplementary Table 0). In addition, participants were asked to complete various surveys in relation to demographics and current and past medical history, medications, smoking history and family history, anthropometry, diet and physical activity as well as stress. Enhanced tests included: OGTT, SSPG, beta-cell function assessment, hsCRP, IgM, cardiovascular imaging (echocardiography, vascular ultrasound), cardiopulmonary exercise, CVD markers and wearable devices (physiology and activity monitor, CGM). In addition, multi-level molecular profiling was performed (emerging tests) including genome, gene expression (transcriptome), immune proteins (immunome), proteins (proteome), small molecules (metabolome) and gut microbes (microbiome). Clinical laboratory measures, immune proteins and cardiovascular biomarkers are detailed in Supplementary Table 0. Participant surveys included the International Physical Activity Questionnaire, Stress and Adversity Inventory and Perceived Stress Scale-10 (refs. [70–72]).

Modified insulin suppression test. Sixty-nine participants underwent the modified insulin suppression test[73] to determine SSPG levels. The test was performed after an overnight fast and consists of 180-min infusion of octreotide ($0.27\,\mu g\,m^{-2}\,min^{-1}$), insulin ($0.25\,\mu g\,m^{-2}\,min^{-1}$) and glucose ($240\,\mu g\,m^{-2}\,min^{-1}$) with blood draws at minutes 150, 160, 170 and 180. The oximetric method was used to determine blood glucose and SSPG was determined by taking the mean of the four measurements. Reasons for not participating in this test included medical contraindications ($n=9$), refusal ($n=5$), dropping out of the study ($n=11$) and not yet performed ($n=15$).

Multi-omics measures. Detailed methods regarding sample preparation, data acquisition and data preprocessing are available in the main NIH integrated Human Microbiome Project study by Zhou et al.[10]. We briefly summarize these methods here.

Genomics. Whole exome sequencing ($n=88$) was performed by an accredited facility and variant calling was performed using an in-house pipeline (HugeSeq)[74]. Exomes were assessed for pathogenic variants according to the American College of Medical Genetics Guidelines[12,75]. The Online Mendelian Inheritance in Man database was used. Further details on processing and variant calling are provided in Rego et al.[12].

PBMC RNA sequencing. RNA sequencing from bulk PBMCs was performed using the TruSeq Stranded total RNA LT/HT Sample Prep Kit (Illumina) and sequenced on Illumina HiSeq 2000 instrument. The TopHat package[76] (v.2.0.11) in R (v.3.4) was used to align the reads to personal genomes, followed by HTseq (v.0.6.1) and DESEQ2 (v.3.5)[77] for transcript assembly and RNA expression quantification.

Plasma sequential window acquisition of all theoretical (SWATH)-mass spectroscopy proteomics. A NanoLC 425 System (SCIEX) was used to separate tryptic peptides of plasma samples. Mass spectroscopy analyses were performed with randomized samples using SWATH Acquisition on a TripleTOF 6600 System equipped with a DuoSpray Source and 25 µm I.D. electrode (SCIEX). A final data matrix was produced with 1% FDR at peptide level and 10% FDR at protein level. Protein abundances were computed as the sum of the three most abundant peptides (top3 method). To address batch effects, subtraction of the principal components showing a major batch bias was performed using Perseus (v.1.4.2.40).

Immune protein measurements. The 62 plex-Luminex antibody-conjugated bead capture assay (Affymetrix) was used to characterize blood levels of immune proteins. The assay was performed by the Stanford Human Immune Monitoring Center. The protocol is available in ref. [78].

Plasma liquid chromatography–mass spectrometry (LC–MS) metabolomics. Untargeted plasma metabolomics was performed using a broad-spectrum LC–MS platform[79]. This analytical platform has been optimized to maximize metabolome coverage and involves complementary reverse-phase liquid chromatography (RPLC) and hydrophilic interaction liquid chromatography (HILIC) separations. Data were acquired on a Q Exactive plus mass spectrometer (Thermo Scientific) for HILIC, and a Thermo Q Exactive mass spectrometer (Thermo Scientific) for RPLC. Both instruments were equipped with a HESI-II probe and operated in full mass-spectroscopy scan mode. Tandem mass spectroscopy data were acquired at various collision energies on pooled samples. LC–MS data were processed using Progenesis QI (Nonlinear Dynamics) and metabolic features were annotated by matching retention time and fragmentation spectra to authentic standards or to public repositories. Some metabolites elute in multiple peaks and were indicated with a number in parenthesis following the metabolite name ordered by elution time.

Plasma lipidomics. Lipids were extracted and analyzed as previously described[80]. Briefly, we used a mixture of methyl tertiary-butyl ether, methanol and water to extract lipids from 40 µl of plasma following biphasic separation. Lipids were then analyzed with the Lipidyzer platform consisting in a DMS device (SelexION Technology, SCIEX) and a QTRAP 5500 (SCIEX). Lipids were quantified using a mixture of 58 labeled internal standards provided with the platform. Lipodomics data is provided in Supplementary Data Table 4.

16S Microbiome sequencing. DNA was extracted from stool in line with the Human Microbiome Project's (HMP) Core Sampling Protocol A (https://www.hmpdacc.org). Targeted rRNA gene amplification of the V1–V3 hypervariable regions of the 16S rRNA gene was performed using primers 27F and 534R (27F: 5′-AGAGTTTGATCCTGGCTCAG-3′ and 534R: 5′-ATTACCGCGGCTGCTGG-3′), and subsequently sequenced using 2×300 base-pair paired-end sequencing (Illumina MiSeq). Illumina's software handles initial processing of all the raw sequencing data. A standard of one mismatch in primer and zero mismatch in barcode was applied to assign read pairs to the appropriate sample in a pool of samples. Barcodes and primers were removed before analysis. Amplicon sequences were clustered and operational taxonomic units picked by Usearch against the GreenGenes database (May 2013 version) and final taxonomic assignment were performed using RDP-classifier.

ASCVD circulating markers. Millipore immunoassays human cardiovascular disease panels 1–4 (HCVD1MAG-67K, HCVD2MAG-67K, HCVD3MAG-67K, HCVD4MAG-67K) were used to characterize blood ASCVD circulating markers. The assays were performed by the Stanford Human Immune Monitoring Center by following the manufacturer's instructions.

Wearable physiology and activity monitoring. Participants wore a Basis watch during the first part of the study and a Fitbit Charge 2 during the last part of the study. We developed a special algorithm, 'Change of Heart', to detect abnormalities in heart rate relative to a person's baseline that was shown to provide an early warning signal of clinical abnormalities and disease, which is described in detail in Li et al.[2].

Continuous glucose monitoring (CGM). CGM was performed with the Dexcom G4 CGM system. Participants wore the monitors for 2–4 weeks with interstitial glucose concentrations recorded every 5 min. They were also given glucose meters (AccCheck Nano SmartView) to measure finger prick blood glucose concentrations twice a day for the purpose of calibration.

Echocardiography. Baseline rest echocardiography was performed using commercially available echo systems (iE33; Philips Medical Imaging). Post-stress images were acquired immediately post-exercise, as per international consensus. Digitized echocardiographic studies were analyzed by the Stanford

Cardiovascular Institute Biomarker and Phenotypic Core Laboratory on Xcelera workstations in accordance with published guidelines of the American Society of Echocardiography[81]. Regarding specific echocardiographic variables, left ventricular ejection fraction was calculated by manual contouring of apical imaging[82]. Left ventricular global longitudinal strain (LV GLS) was calculated from triplane apical imaging on manual tracings of the mid-wall with the formula for Lagrangian strain (%) = 100 × (L1 − L0)/L0), as previously described[83]. With tissue Doppler imaging, we used peak myocardial early diastolic velocity at the lateral mitral annulus and the assessment of trans mitral to tissue Doppler imaging early diastolic velocity ratio (E/e')[84,85].

Vascular ultrasound. Screening for subclinical atherosclerosis was performed using vascular ultrasound of the carotid and femoral artery using a 9.0 MHz Philips linear array probe and iE33 xMATRIX echocardiography System manufactured by Philips. Vascular stiffness was assessed using central pulse wave velocity (PWV).

Cardiopulmonary exercise testing. Symptom-limited cardiopulmonary exercise ventilatory expired gas analysis was completed with an individualized RAMP treadmill protocol[86]. Participants were encouraged to exercise to maximal exercise capacity. In addition, we monitored the respiratory exchange ratio during exercise and considered an respiratory exchange ratio <1.05 as representing suboptimal or limitations associated with fatigue. Ventilatory efficiency, oxygen consumption (VO_2), volume of carbon dioxide production (VCO_2) and other cardiopulmonary exercise variables were acquired breath by breath and averaged over 10 s intervals using CareFusion Oxygen Pro or CosMEd Quark metabolic system. Ventilatory efficiency and VCO_2 responses throughout exercise were used to calculate the ventilatory efficiency/VCO_2 slope via least squares linear regression ($y = mx + b$, where m is the slope)[87]. Percentage predicted maximal oxygen consumption was derived using the Fitness Registry and the Importance of Exercise: a National Database (FRIEND) registry equation, derived from a large cohort of healthy US individuals who completed cardiopulmonary exercise testing[88].

iPOP participant surveys. Participants completed a survey on how the study had affected their eating and exercise habits, what they learned about their health during the study, whether they discussed findings with their doctor, any follow-up testing and other people they shared data with. This survey was initially administered anonymously but we then switched to surveys identified by participant identity. The quantitative results reported in Fig. 6 are from all participants who filled out an identifying survey (using the last filled out survey where there was more than one). We used participant comments from anonymous and identified surveys in Supplementary Table 27. At each quarterly visit, participants were asked about changes to health and medication. Participants were also asked by the study dietician how iPOP participation and CGM monitoring affected their health behaviors (Supplementary Table 28).

Calculation of insulin secretion rates (ISR) and disposition index. We used the ISEC program[89] to calculate the ISR from deconvolution of C-peptide measurements from plasma sampled at various time points during the OGTT (at minutes 0, 30 and 120). The deconvolution method uses population-based kinetic parameters[15] for C-peptide clearance to estimate ISRs at other time points. ISR was reported in pmol kg^{-1} min^{-1} at every 15-min time interval between 0 and 120 minutes. The disposition index was calculated as the ISR at 30 min (ISR30) times the Matsuda index, which was calculated as in Cersosimo et al.[14]. Disposition index was reported as (pmol kg^{-1} min^{-1})/(mg ml^{-1} × μU ml^{-1}).

Cluster analysis and association of disposition index with multi-omics measures. ISRs were row standardized across the nine time points from an OGTT sample and then clustered via the k-means clustering algorithm in R (v.3.5) (function 'kmeans'), with $k = 4$. Simple linear models were used to associate the disposition index with each multi-omics analyte. Values for multi-omics analytes were from the time point closest to the OGTT date. Adjustment of P values for multiple testing was performed using the Benjamini–Hochberg method, with an adjusted $P < 0.10$ used to identify analytes significantly associated with the disposition index.

ASCVD and adjusted ASCVD risk score calculation. The ASCVD pooled cohort risk equations were implemented according to the instructions in the 2013 ACC/AHA Guideline on the Assessment of Cardiovascular Risk[34], using SAS v.9.4 statistical software. The baseline time point was used for all participants except those that turned 40 during the study. In these cases, the first time point after age 40 was chosen. Participants under the age of 40 ($n = 7$) for the entire duration of the study were assigned the age of 40 for the purposes of ASCVD risk score calculation. To calculate the optimal risk for someone of a particular, age, sex and race, we used total cholesterol of 170, HDL of 50, and systolic blood pressure of 110 with no blood pressure medications, diabetes or smoking. Adjusted ASCVD risk score was calculated by subtracting the optimal ASCVD risk score for a person of the same age, sex and race, from the participant's ASCVD risk score.

Association of multi-omic analytes and adjusted ASCVD risk score. First, a median value was calculated for each analyte in each participant using healthy time points. A minimum of three healthy visits per participant was required. Spearman correlations were then calculated between adjusted ASCVD risk score and the median value of each multi-omics analyte. Associations were considered significant for analytes with $q < 0.2$. FDR correction was performed using the 'qvalue' package (v.1.36.0) in R (v.3.0.1).

Correlation network analysis. Spearman correlations among molecules significantly associated with disposition index and adjusted ASCVD risk score were calculated using the rcorr function in the 'Hmisc' package (v.3.15-0) in R (v.3.0.1) and P values were corrected for multiple hypothesis using Bonferroni. Correlation networks were plotted using the R package 'igraph' (v.0.7.1) and the layout used was Fruchterman–Reingold. Edges represent correlations with Bonferroni-corrected $P < 0.05$ and 0.10 for the disposition index and ASCVD risk score, respectively.

Linear mixed models (healthy-baseline and dynamic models). SAS v.9.4 Proc Mixed was used to perform linear mixed model analysis using the full maximum likelihood method of estimation and the between-within method for estimating degrees of freedom. We used a random intercept model with an unstructured covariance matrix for all analytes. Since linear time explained only a small amount of within-person variation in FPG (1.2%) and HbA1C (5.0%) at healthy time points, we did not include time in our models. The outcome measures (FPG, HbA1C and hsCRP) were log transformed in all models and the analytes were standardized to a mean of zero and standard deviation of one. All models were controlled for sex and age at consent. The healthy-baseline models used data from healthy quarterly visits. The dynamic analysis used the ratio to the first available time point for each outcome measure and analytes and used all time points in the study. P values were corrected for multiple hypothesis testing using the Benjamini–Hochberg procedure. Significant analytes have Benjamini–Hochberg FDR < 0.2.

Data reporting. In reporting results we considered consistency between models and results, validation through literature review of emerging molecules and relevance to disease state or risk condition. We also considered whether differing results varied because of sensitivity and variability of measures, the difference between evaluating absolute baseline values versus relative change and the potential for biological saturation.

Multi-omics outlier analysis. Z scores (mean of zero and standard deviation of one) were calculated after $\log_2$-transformation for all measures in all participants and outliers were defined as absolute $Z >$ ninety-fifth percentile. Associated P values were calculated assuming a normal distribution. P values were corrected for multiple hypothesis using the Benjamini–Hochberg procedure.

Stroke genes outlier analysis. Z scores were calculated as described above for 14 of 32 genes recently identified as being associated with stroke and stroke types[40]. The 14 genes that we detected in our RNA-seq dataset were as follows: *CASZ1*, *CDK6*, *FURIN*, *ICA1L*, *LDLR*, *LRCH1*, *PRPF8*, *SH2B3*, *SH3PXD2A*, *SLC22A7*, *SLC44A2*, *SMARCA4*, *ZCCHC14* and *ZFHX3*. A composite Z score was calculated by summing the individual gene Z scores.

Pathway enrichment analysis. The web tool IMPaLA v.11 (build April 2018; integrated molecular pathway-level analysis, http://impala.molgen.mpg.de) was used for the joint pathway analysis of proteins (from SWATH–MS) and metabolites (from LC–MS) abundances. Uniprot and HMDB accession numbers were used for proteins and metabolites, respectively. Pathway significance for proteins and metabolites separately was calculated using a hypergeometric test; the whole space of proteins and metabolites described in the pathways were used as a background. Joint P values combining protein and metabolite pathways are calculated using Fisher's method. Multiple comparisons are controlled for using the Benjamini–Hochberg procedure[90].

Exercise sub-study analysis. ASCVD risk scores were calculated using cholesterol laboratory results closest to the exercise study date using the same method as that used for the baseline ASCVD risk scores. Correlation analysis was done with 'corrplot' package in R (v.3.3.2). The network was plotted using Cytoscape v.3.4.0 (ref. [91]), where edges represent correlations with statistically significant Spearman's values (FDR < 0.2). False discovery rate correction was performed using the 'qvalue' package (v.1.36.0) in R. The distance between nodes represents the strength of the pull between a node and its connected neighbors. The larger the value, the closer the distance between the two nodes. The system was iterated until dynamic equilibrium using the prefuse force directed layout[92].

Microbiome diversity: univariate models. Shannon diversity was calculated with SAS v.9.4 using a code adapted from Montagna[93]. SAS v.9.4 Proc Mixed using a restricted maximum likelihood estimation of the between–within degrees of freedom method was used to model the association of HbA1c, FPG and SSPG and Shannon diversity H' index. Preliminary analyses were done in Proc Gam and suggested an 'inverse u' distribution for all three measures in relationship to the Shannon diversity index. HbA1C and FPG were modeled using a repeated

measures model with spatial power covariance structure. Shannon was entered into the model as a quadratic predictor of HbA1C and FPG. SSPG was modeled slightly differently because SSPG was only measured once in participants thus models with the predictor SSPG included Shannon diversity in the random statement. In addition, Shannon diversity as a quadratic term did not improve model fit and was not significant in any SSPG models so we present only the models with Shannon as a linear predictor (Supplementary Table 6).

Microbiome diversity: multivariate model. For our multivariate model (SAS v.9.4 Proc Mixed), the full maximum likelihood method of estimation was used to enable comparison between models. The degree of freedom method was the between-within method. We used an unstructured covariance matrix for the models presented. In addition to the models presented in Supplementary Table 7, we also evaluated the effect of adding baseline BMI, consent age or metformin use to the model. None of these covariates added significantly to the model and thus were left out of subsequent models. In addition, we evaluated whether use of the Firmicutes/Bacteroidetes ratio in place of the phylum Bacteroidetes proportion would improve the model. However, the ratio accounted for substantially less within-person variation in Shannon diversity (10.4%) thus we kept the proportion of the phylum Bacteroidetes in the final model.

Modeling individual Shannon diversity trajectories. We modeled the change in Shannon diversity over time for individual participants using a general additive model (SAS Proc Gam) that separates the linear and non-linear components of the trajectory. The *F*-test of the model using time as a predictor of Shannon diversity was compared to the null model and was calculated according to SAS usage note 32927: http://support.sas.com/kb/32/927.html (accessed March 2018).

SSPG and OGTT prediction models. *Reprocessing of microbiome data.* For the prediction models, the microbiome 16S reads were reprocessed using QIIME 2 (ref. [94]) (https://qiime2.org) and the DADA2 (ref. [95]) denoising plugin. The resulting read depth was 18,885 ± 11,852 (mean ± s.d.) following paired-end joining, removal of chimeric reads and removal of samples with <7,000 read depth. Taxonomic assignment was carried out using a naïve Bayes classifier trained on the above primers with the 99% 13_8 GreenGenes operational taxonomic unit dataset as reference sequences[96]. DADA2 facilitates cross-study comparison by providing DNA sequences of features thus making it more appropriate for prediction models that will eventually need further external validation[97].

Feature selection. Features from multi-omics (clinical laboratory results, transcriptome, immunome, proteome, metabolome, lipidome and microbiome) were standardized to zero mean with unit variance. Clinical laboratory (including SSPG), immunome and metabolomics data was log transformed before standardization. The variance stabilizing transformation had been used for RNA-seq data. The sample IDs used for each SSPG and OGTT model are provided in Supplementary Data Tables 5–24. We then used the 'MXM' R package[27] (v.0.9.7) with the Max-Min Parents and Child algorithm (MMPC)[26] option to identify features that are parents or children of SSPG in a Bayesian network constructed from all the available data. The features selected by the algorithm are hypothesized to be direct causes or effects of SSPG in the data, as each feature selected are SSPG dependent when conditioned on every possible subset of the other features. These features provide novel information about SSPG and are thus most useful for prediction. There were 41 participants with SSPG values and all multi-omics data. Feature selection was performed using leave-one-out cross validation, where 41 training sets were constructed and each training set excluded the data from a different patient. We ran the MMPC algorithm on each training set. Features that were identified by the MMPC algorithm in ≥20% of training sets were used as features in the model. For the OGTT predictive model, there was no lipidomics data available.

Ridge regression. Ridge regression was performed using R (v.3.4.1). For each -ome, we used the sample at the closest time point that was equal or before the time point of the patient's SSPG/OGTT measurement. We performed leave-one-out cross validation to maximize available training data. For each training set, we optimized the hyperparameter by performing a grid search and selecting the model that minimizes test error. The predicted SSPG/OGTT value was the value from the cross-validation iteration in which that SSPG/OGTT data point and its associated features were excluded from the training set. We used these predicted values to calculate MSE and R^2 values. The value of the hyperparameter used was the average of the hyperparameters that minimized test error during cross validation.

Ethnicity principal components analysis (PCA) plot. Ethnicity information for 72 individuals in the study was broadly classified into the five 1,000GP Consortium super-population definitions, which are, namely, African (AFR), East Asian (EAS), European (EUR), South Asian (SAS) and admixed American (AMR). Individuals who self-identify as Indians from South Asia were categorized as SAS ($n=7$), Hispanics and Latinos as AMR ($n=3$), East Asians as EAS ($n=8$), Caucasians as EUR ($n=50$) and African Americans ($n=4$) as AFR. The ethnicity information from the 2,504 samples, definitions of the populations and super-populations and genetic information of the 1,000GP were obtained from ftp://ftp.1000genomes.ebi.ac.uk/vol1/ftp/release/20130502/ (downloaded in April 2017).

The following filters were first implemented for each individual genome for the study: (1) we removed indels, leaving only the single-nucleotide variants (SNVs), (2) we removed SNVs without the 'PASS' tag, (3) we kept SNVs with a minimum read depth of 1 and (4) we removed SNVs with missing genotypes. We then intersected the genetic loci from 72 individuals and the samples from the 1,000GP to obtain 6,653 SNVs common to both datasets. To reduce the chance of linkage disequilibrium and dependency between SNVs due to close proximity, we further thinned out the SNV set by taking every third SNV. Finally, we had a combined set of 2,576 samples and 2,318 SNVs that we used for PCA. We used the smartpca tool in the PLINK2 suite to generate the PCA[98].

Reporting Summary. Further information on research design is available in the Nature Research Reporting Summary linked to this article.

Data availability

Raw omics data (transcriptome, immunome, proteome, metabolome, microbiome) included in this study are hosted on the NIH Human Microbiome 2 project site (https://portal.hmpdacc.org/) under the T2D project along with clinical laboratory data to 2016. Data from participants who have not consented to make their data public are available on dbGAP (accession phs001719.v1.p1). Additional data unique to this manuscript has been provided in the Supplementary Data files.

References

69. The Integrative Human Microbiome Project. Dynamic analysis of microbiome-host omics profiles during periods of human health and disease. *Cell Host Microbe* **16**, 276–289 (2014).
70. Cohen, S. & Williamson, G. in *The Social Psychology of Health* (eds Spacapan, S. and Oskamp, S.) 31–67 (Sage Publications, 1988).
71. Slavich, G. M. & Shields, G. S. Assessing lifetime stress exposure using the Stress and Adversity Inventory for adults (Adult STRAIN): an overview and initial validation. *Psychosom. Med.* **80**, 17–27 (2018).
72. Lee, P. H., Macfarlane, D. J., Lam, T. H. & Stewart, S. M. Validity of the international physical activity questionnaire short form (IPAQ-SF): a systematic review. *Int. J. Behav. Nutr. Phys. Act.* **8**, 115 (2011).
73. Pei, D., Jones, C. N. O., Bhargava, R., Chen, Y.-D. I. & Reaven, G. M. Evaluation of octreotide to assess insulin-mediated glucose disposal by the insulin suppression test. *Diabetologia* **37**, 843–845 (1994).
74. Lam, H. Y. K. et al. Detecting and annotating genetic variations using the HugeSeq pipeline. *Nat. Biotechnol.* **30**, 226–229 (2012).
75. Kalia, S. S. et al. Recommendations for reporting of secondary findings in clinical exome and genome sequencing, 2016 update (ACMG SFv2.0): a policy statement of the American College of Medical Genetics and Genomics. *Genet. Med.* **19**, 249–255 (2017).
76. Trapnell, C., Pachter, L. & Salzberg, S. L. TopHat: discovering splice junctions with RNA-Seq. *Bioinformatics* **25**, 1105–1111 (2009).
77. Love, M. I., Huber, W. & Anders, S. Moderated estimation of fold change and dispersion for RNA-seq data with DESeq2. *Genome Biol.* **15**, 1–21 (2014).
78. *Luminex Multiplex Analysis* (Stanford Human Immune Monitoring Core, 2018); http://iti.stanford.edu/content/dam/sm/iti/documents/himc/protocols/LuminexMultiplexAnalysisprotocol030213.doc
79. Contrepois, K., Jiang, L. & Snyder, M. Optimized analytical procedures for the untargeted metabolomic profiling of human urine and plasma by combining hydrophilic interaction (HILIC) and reverse-phase liquid chromatography (RPLC)-mass spectrometry. *Mol. Cell. Proteomics* **14**, 1684–1695 (2015).
80. Contrepois, K. et al. Cross-platform comparison of untargeted and targeted lipidomics approaches on aging mouse plasma. *Sci. Rep.* **8**, 17747 (2018).
81. Lang, R. M. et al. Recommendations for cardiac chamber quantification by echocardiography in adults: an update from the American Society of Echocardiography and the European Association of Cardiovascular Imaging. *J. Am. Soc. Echocardiogr.* **28**, 1–39.e14 (2015).
82. Wilson, P. W. F. et al. Prediction of coronary heart disease using risk factor categories. *Circulation* **97**, 1837–1847 (1998).
83. Smith, D. A. In adults without CVD, the MESA score, including coronary artery calcium, predicted 10-y risk for CHD events. *Ann. Intern. Med.* **164**, JC35 (2016).
84. McClelland, R. L. et al. 10-Year coronary heart disease risk prediction using coronary artery calcium and traditional risk factors: derivation in the mesa (multi-ethnic study of atherosclerosis) with validation in the HNR (Heinz Nixdorf Recall) study and the DHS (Dallas Heart Study). *J. Am. Coll. Cardiol.* **66**, 1643–1653 (2015).
85. Lee, K. K., Cipriano, L. E., Owens, D. K., Go, A. S. & Hlatky, M. A. Cost-effectiveness of using high-sensitivity C-reactive protein to identify intermediate- and low-cardiovascular-risk individuals for statin therapy. *Circulation* **122**, 1478–1487 (2010).

86. Myers, J., Bader, D., Madhavan, R. & Froelicher, V. Validation of a specific activity questionnaire to estimate exercise tolerance in patients referred for exercise testing. *Am. Heart J.* **142**, 1041–1046 (2001).
87. Arena, R., Myers, J., Aslam, S. S., Varughese, E. B. & Peberdy, M. A. Technical considerations related to the minute ventilation/carbon dioxide output slope in patients with heart failure. *Chest* **124**, 720–727 (2003).
88. Kaminsky, L. A., Imboden, M. T., Arena, R. & Myers, J. Reference standards for cardiorespiratory fitness measured with cardiopulmonary exercise testing using cycle ergometry: data from the fitness registry and the importance of exercise national database (FRIEND) Registry. *Mayo Clin. Proc.* **92**, 228–233 (2017).
89. Hovorka, R., Soons, P. A. & Young, M. A. ISEC: a program to calculate insulin secretion. *Comput. Methods Programs Biomed.* **50**, 253–264 (1996).
90. Kamburov, A., Cavill, R., Ebbels, T. M. D., Herwig, R. & Keun, H. C. Integrated pathway-level analysis of transcriptomics and metabolomics data with IMPaLA. *Bioinformatics* **27**, 2917–2918 (2011).
91. Shannon, P. et al. Cytoscape: a software environment for integrated models of biomolecular interaction networks. *Genome Res.* **13**, 2498–2504 (2003).
92. Fruchterman, T. M. J. & Reingold, E. M. Graph drawing by force-directed placement. *Softw. Pract. Exp.* **21**, 1129–1164 (1991).
93. Montagna, P. A. Using SAS to manage biological species data and calculate diversity indices. in *2014 SCSUG Educational Forum* (South Central SAS Users Group, 2014).
94. Caporaso, J. G. et al. QIIME allows analysis of high-throughput community sequencing data. *Nat. Methods* **7**, 335–336 (2010).
95. Callahan, B. J. et al. DADA2: High-resolution sample inference from Illumina amplicon data. *Nat. Methods* **13**, 581–583 (2016).
96. Bokulich, N. A. et al. Optimizing taxonomic classification of marker-gene amplicon sequences with QIIME 2's q2-feature-classifier plugin. *Microbiome* **6**, 90 (2018).
97. Callahan, B. J., McMurdie, P. J. & Holmes, S. P. Exact sequence variants should replace operational taxonomic units in marker-gene data analysis. *ISME J.* **11**, 2639 (2017).
98. Chang, C. C. et al. Second-generation PLINK: rising to the challenge of larger and richer datasets. *Gigascience* **4**, 7 (2015).

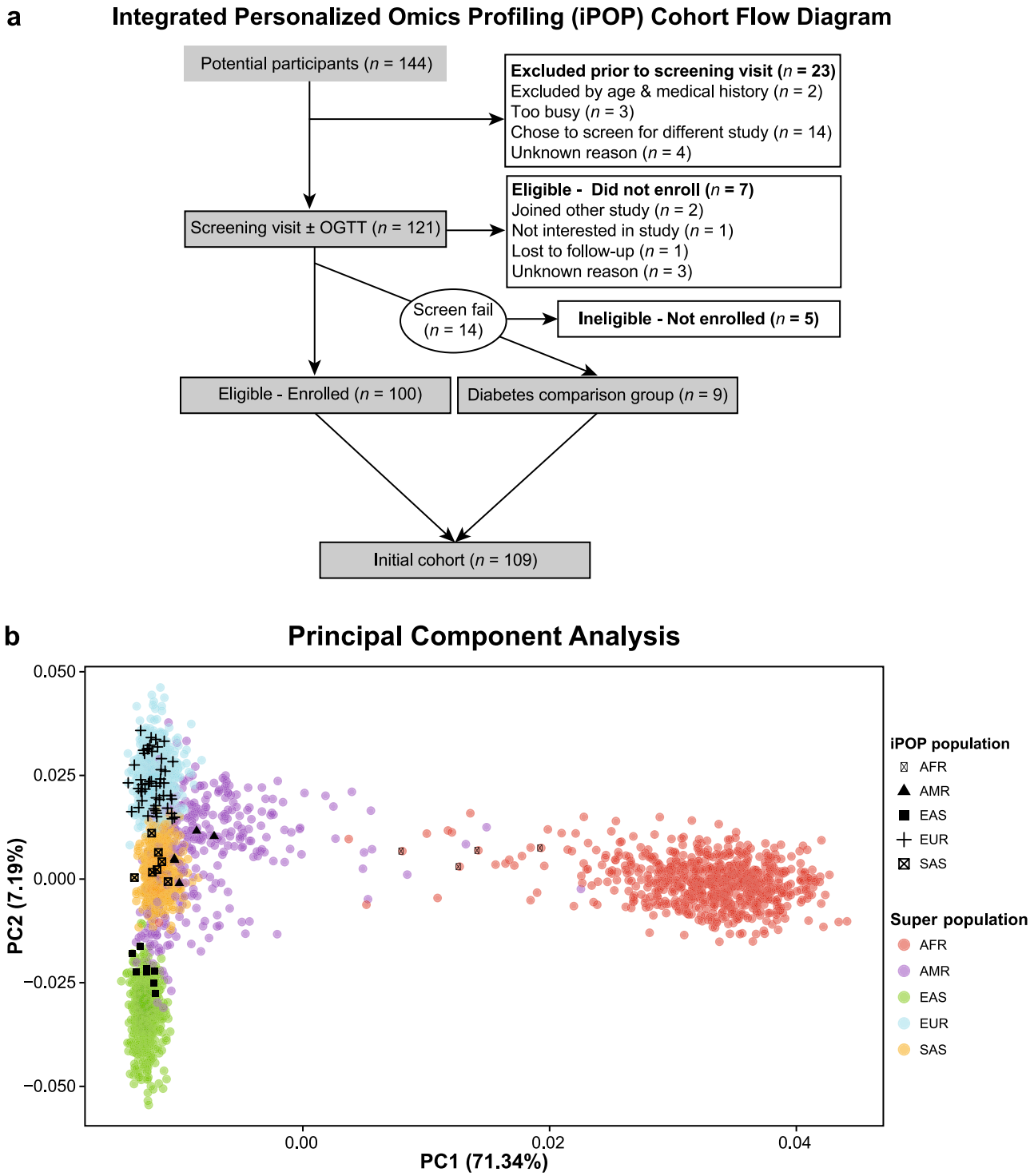

Extended Data Fig. 1 | Integrated personalized omics profiling cohort flow chart and genetic ancestry. a, The flow chart demonstrates recruitment and enrollment of the iPOP cohort. **b**, PCA plot showing the ancestries of 72 participants. The reference includes 2,504 samples from the 1,000GP[11]. Each filled circle is a 1,000GP sample, colored by the super-population of ancestral origin, namely African (AFR; red), admixed American (AMR; purple), East Asian (EAS; green), European (EUR; cyan) and South Asian (SAS; orange). Each black symbol is an individual from the study, which we categorized by self-reported ethnicity consistent with the 1,000GP super-population definitions, namely AFR (black filled circle), AMR (black filled triangle), EAS (black filled square), EUR (black plus sign) and South Asian (a checked box). We see that the individuals in our study have self-reported ancestries generally clustering in the super-population reference panel from the 1,000GP.

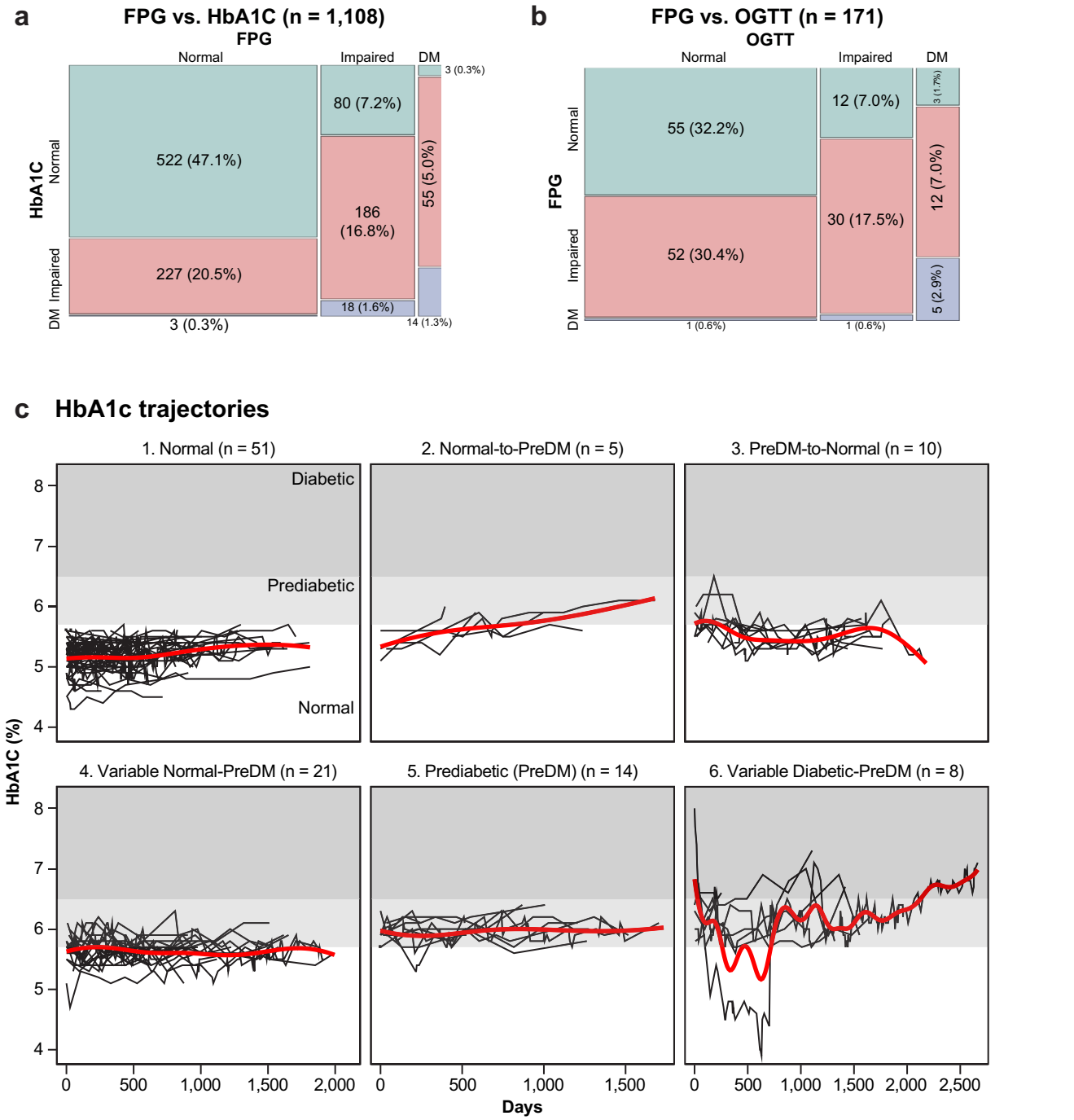

Extended Data Fig. 2 | Comparison of diabetic metrics in categorizing individuals when performed at the same time and HbA1C trajectories. **a**, Overlap of FPG and hemoglobin A1C (HbA1C) categories when simultaneously measured. FPG impaired: 1.0 mg ml^{-1} ≤ FPG < 1.26 mg ml^{-1}; diabetic range: FPG ≥ 1.26 mg ml^{-1}; HbA1C impaired: 5.7% ≤ HbA1C < 6.5%; diabetic range: HbA1C ≥ 6.5%. **b**, Overlap of FPG and 2-hour OGTT when simultaneously measured. FPG ranges as above. OGTT impaired: 1.40 mg ml^{-1} ≤ OGTT < 2.00 mg ml^{-1}; diabetic range ≥2.00 mg ml^{-1}. **c**, Longitudinal patterns of changes in Hemoglobin A1C (HbA1C) over time. Six different patterns could be characterized including: 1, participants who remained in the normal range the entire study (Group 1, $n = 51$); 2, participants who progressed from normal to prediabetic (Group 2, $n = 5$); 3, participants who went from prediabetic to normal (Group 3, $n = 10$); 4, participants whose HbA1C went back and forth from normal to prediabetic (Group 4, $n = 21$); 5, participants whose HbA1C laboratory results were predominantly in the prediabetic range (Group 5, $n = 14$) and 6, participants whose HbA1C crossed into the diabetic range (Group 6, $n = 8$). The red lines represent the overall penalized b-spline of participants' data in each category.

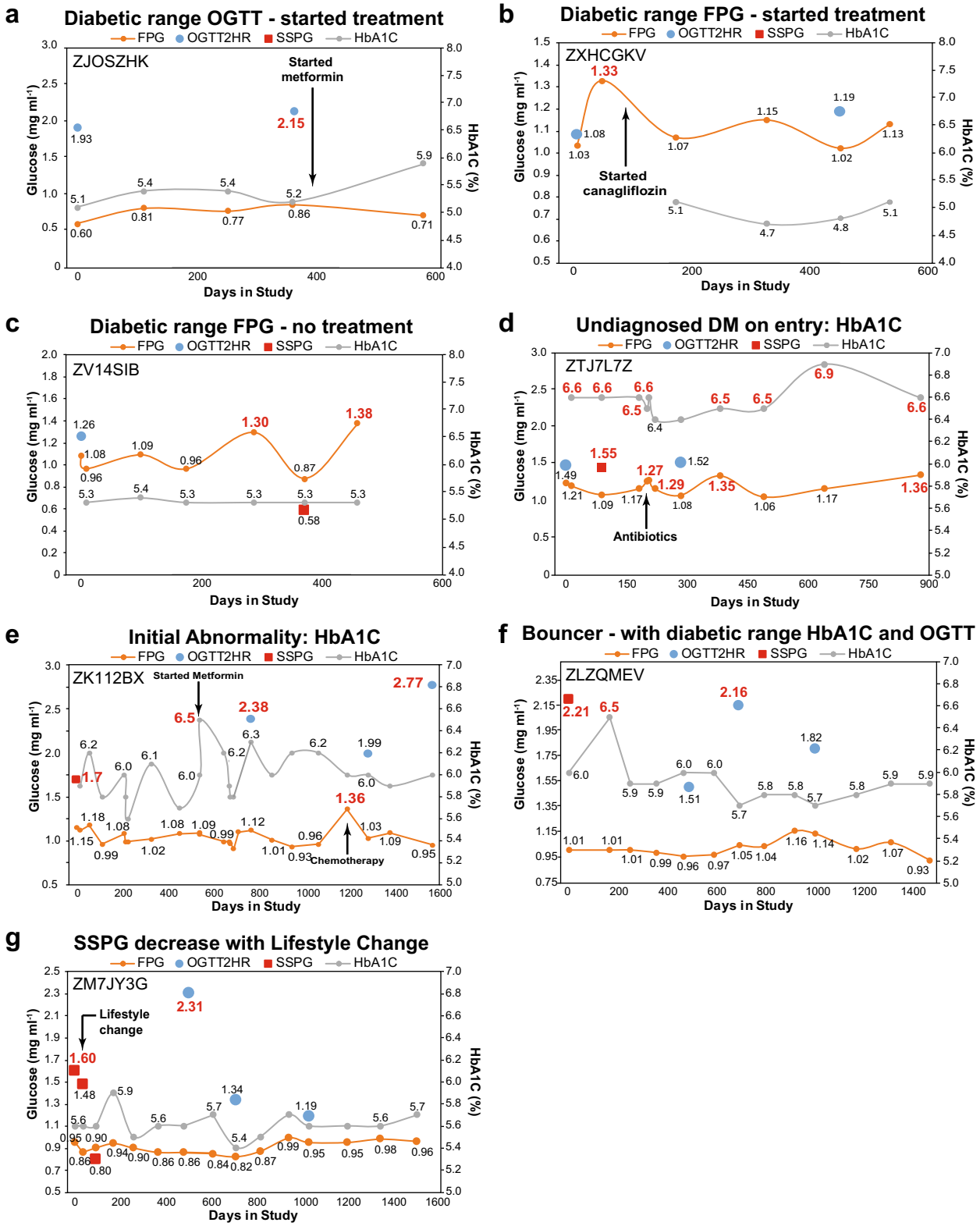

Extended Data Fig. 3 | Additional individual longitudinal trajectories for diabetic measures. Diabetic-range metrics are indicated in red. **a**–**e**, Diabetic-range OGTT (**a**), Diabetic-range FPG (**b**,**c**), undiagnosed DM at study entry (HbA1C) (**d**), Initial abnormality HbA1C (**e**). Note this person had two HbA1C measurements on the same day at two different laboratories and was started on medication based on the higher measurement. **f**,**g**, Bouncer with diabetic-range HbA1C and OGTT (**f**) and SSPG decrease with lifestyle change (**g**).

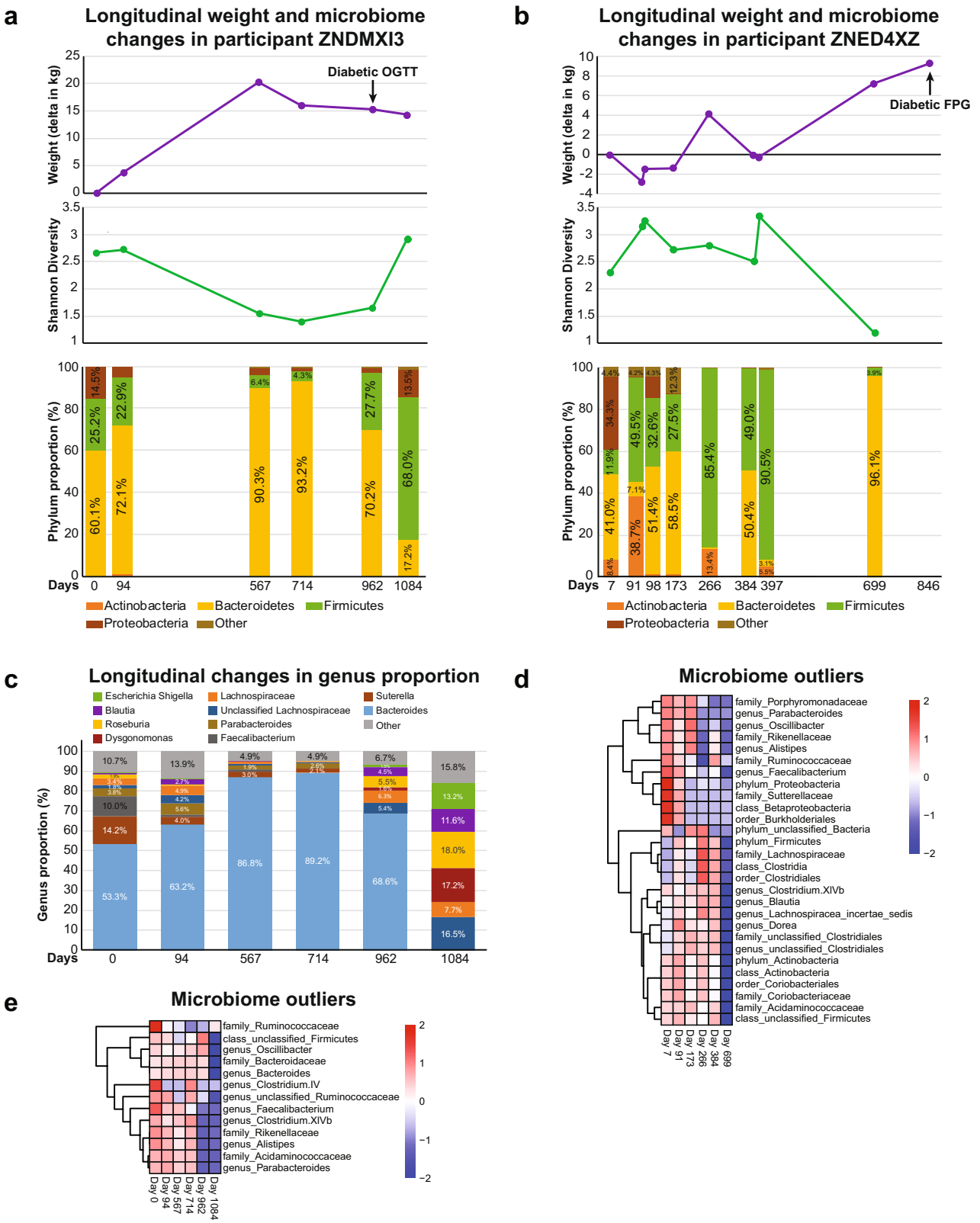

Extended Data Fig. 4 | Longitudinal microbiome trajectories in diabetes. a,**b**, Longitudinal weight, gut microbial Shannon diversity and phylum proportion changes in participants ZNDMXI3 (**a**) and ZNED4XZ (**b**). **c**, Longitudinal changes in genus proportion (ZNDMXI3). **d**,**e**, Microbiome outliers (95th percentile) at the latest microbiome sample time point in participants ZNDMXI3 (**d**) and ZNED4XZ (**e**). Microbial abundance is scaled by row with low (blue) and high (red) abundance.

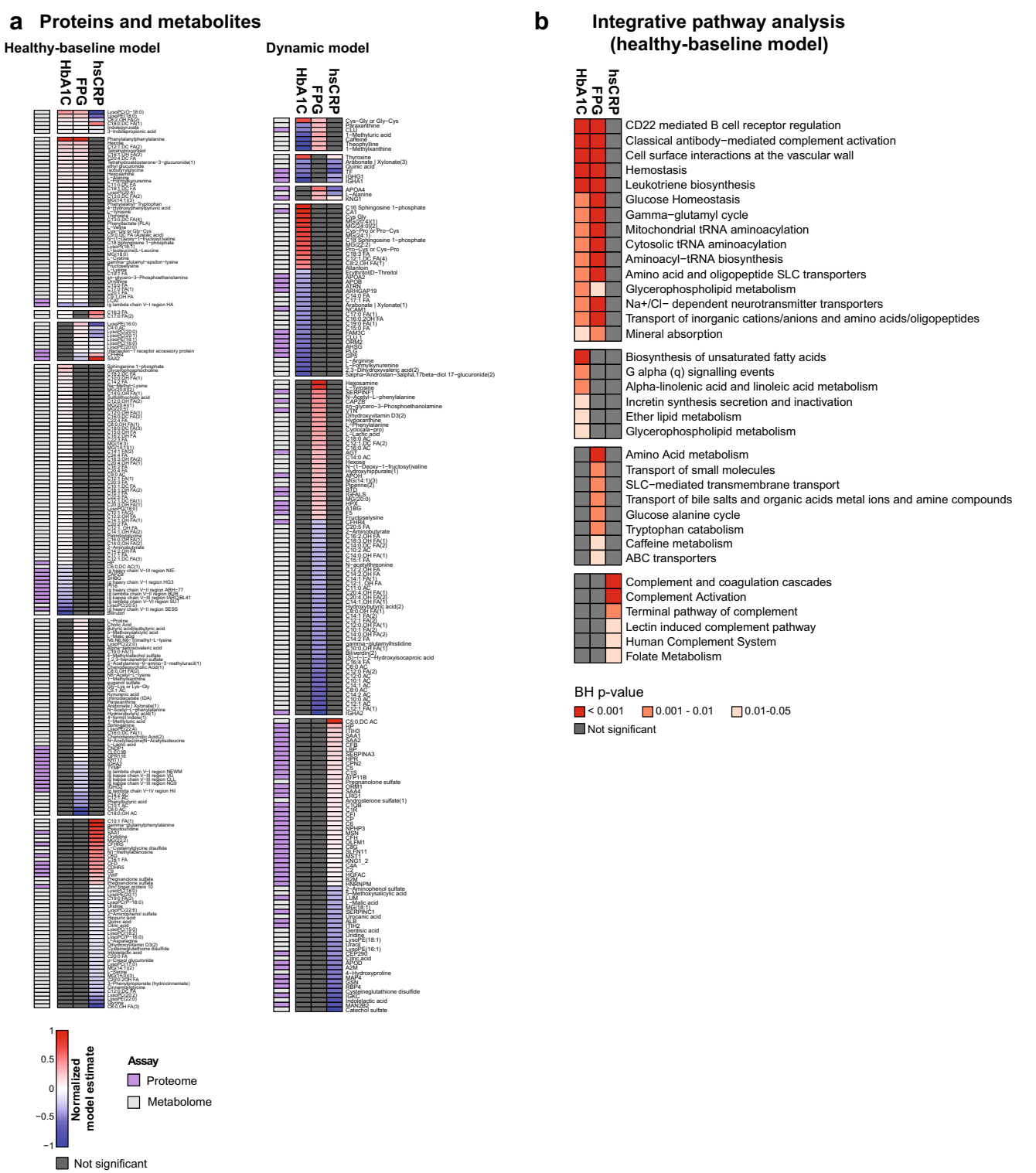

Extended Data Fig. 5 | Multi-omics of glucose metabolism and inflammation. a, Proteins and metabolites associated with HbA1C, FPG and hsCRP using healthy-baseline and dynamic linear mixed models. Healthy-baseline models (HbA1C $n=101$, samples 560; FPG $n=101$, samples 563; hsCRP $n=98$, samples 518) account for repeated measures at healthy time points. Dynamic models are similar models except that analytes are normalized across individuals to the first measurement and all time points in the study are used (HbA1C $n=94$, samples = 836; FPG $n=94$, samples = 843; hsCRP $n=92$, samples 777). Individual analyte P values were determined using a two-sided t-test. Multiple testing correction was performed and molecules were considered significant when Benjamini–Hochberg FDR < 0.2. Model estimates were normalized in each condition so the maximum value equal to 1 and the minimal value equal to −1. **b**, Integrative pathway analysis using IMPaLa[67] of proteins and metabolites associated with HbA1C ($n=101$, samples 560), FPG ($n=101$, samples 563) and hsCRP ($n=98$, samples 518) as determined by the healthy-baseline models (Benjamini–Hochberg FDR < 0.2 at molecule level) that matched to known pathways. Significance of pathways for proteins and metabolites separately is determined by the hypergeometric test (one-sided) followed by Fisher's combined probability test (one-sided) to determine combined pathway significance (Benjamini–Hochberg FDR < 0.05; n's of proteins and metabolites for each pathway are provided in Supplementary Tables 9, 11 and 13).

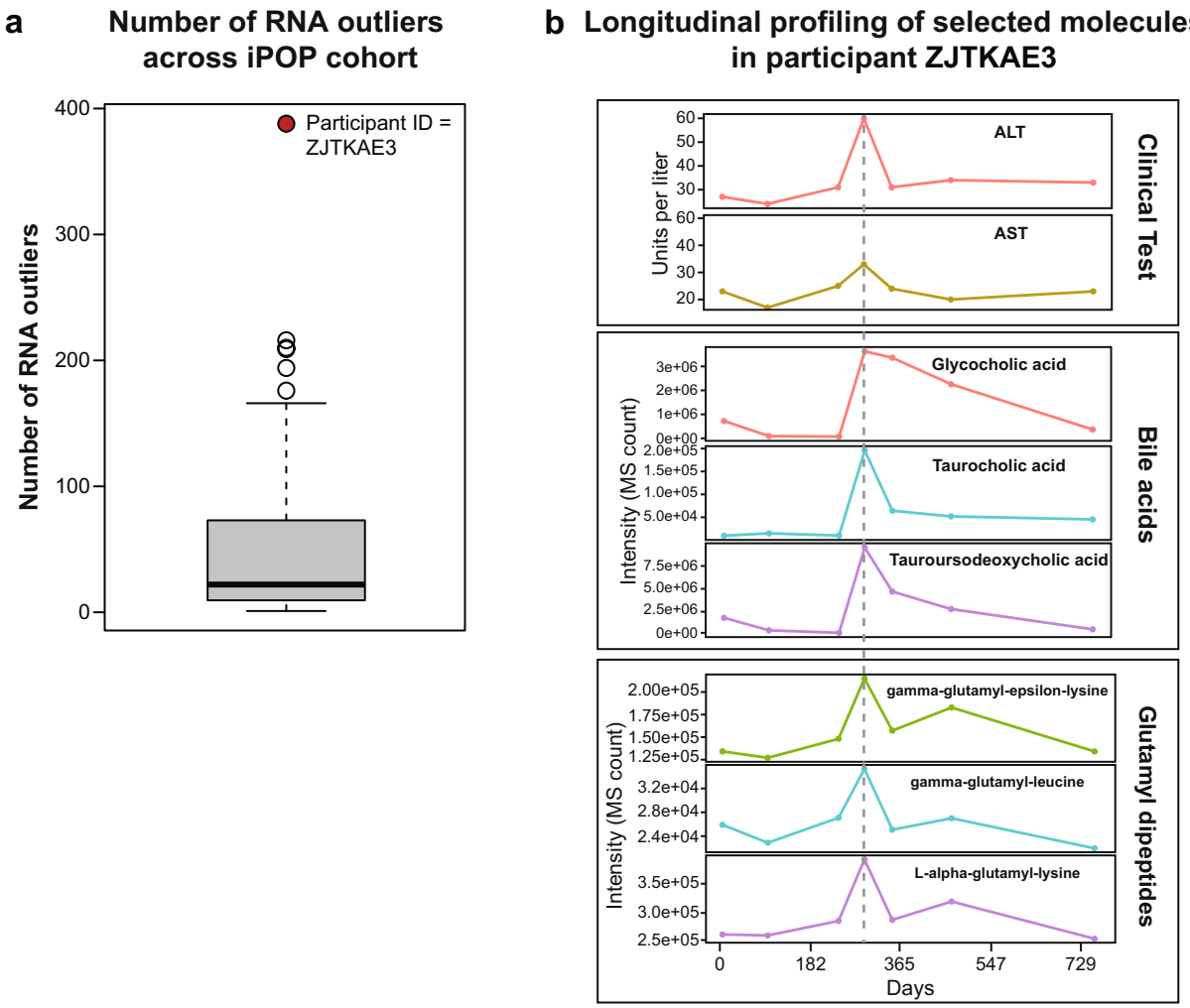

Extended Data Fig. 6 | Outlier Analysis of RNA-seq data. a, Number of outlier RNA molecules (95th percentile) in each participant. Outlier analysis was performed on *Z* scores calculated on the median expression level of each gene at healthy visits in individuals with at least three healthy visits ($n = 63$). The box is defined as 25th and 75th quartile. The upper whisker extends to 1.5 times the interquartile range from the box and the lower whisker to the lowest data point. The horizontal bar in the box is the median value. **b**, Selected clinical laboratory and metabolite trajectories (seven measurement time points) for participant ZJTKAE3 showing a concomitant increase of bile acids and glutamyl dipeptides with ALT (alanine aminotransferase) and AST (aspartate aminotransferase).

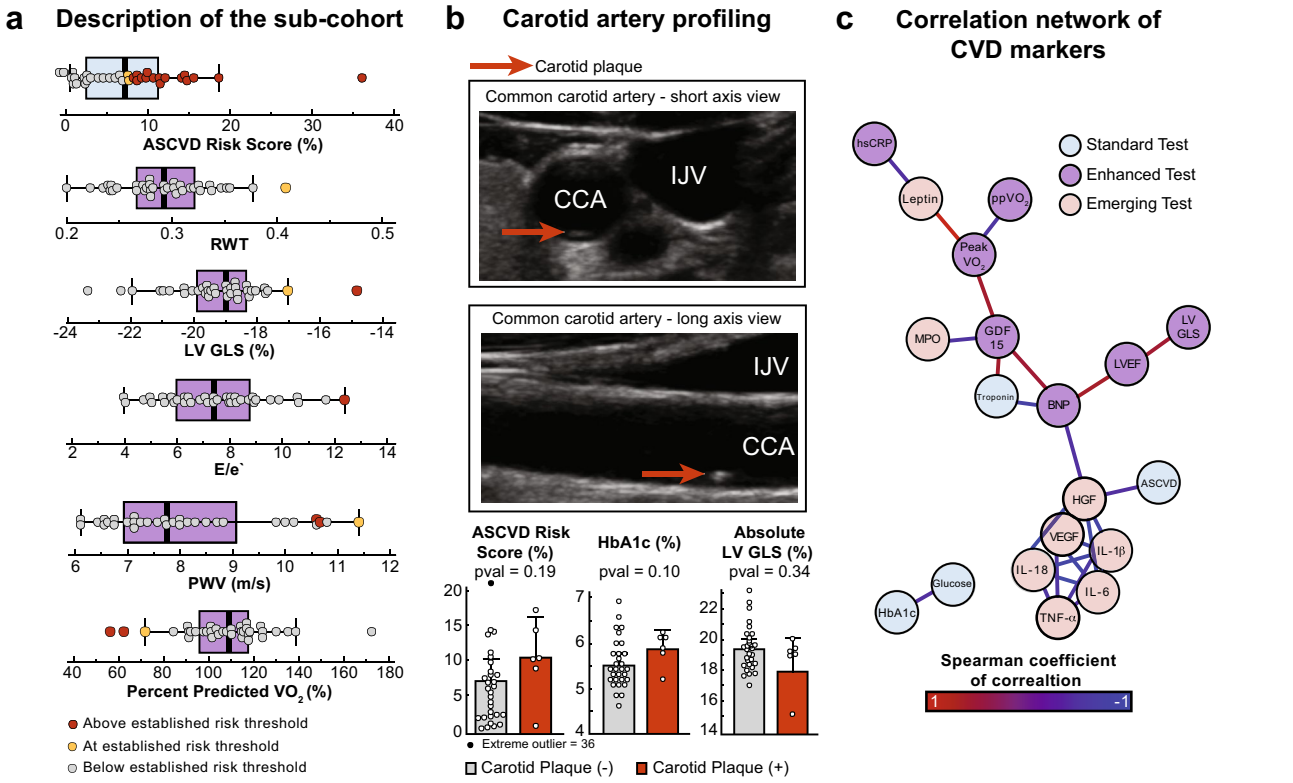

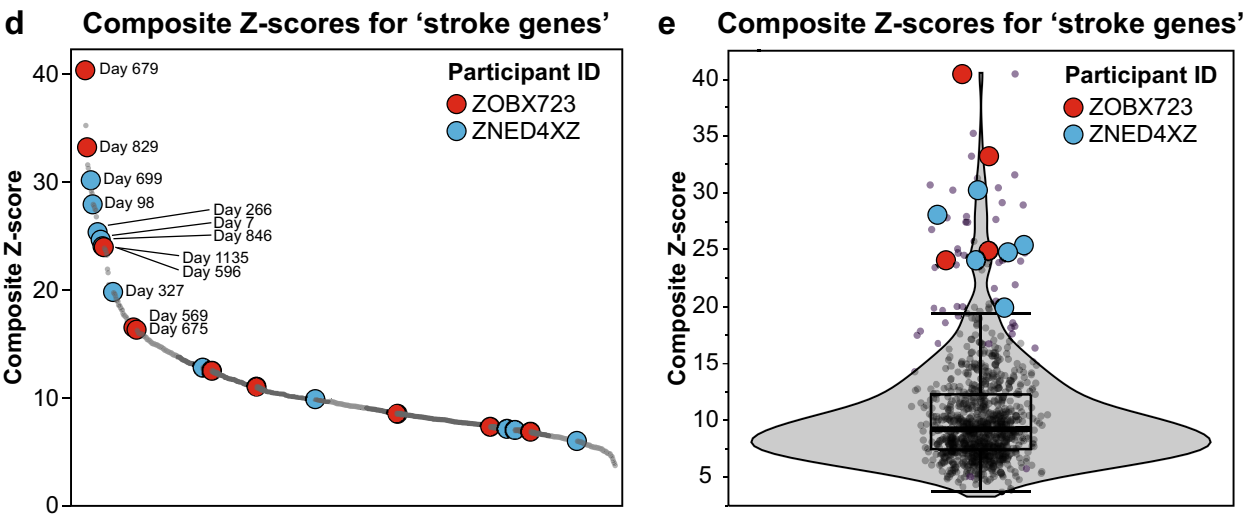

Extended Data Fig. 7 | Multidimensional cardiac risk assessment. a, Distribution of ASCVD risk scores ($n=35$ participants, 36 measurements) and cardiovascular imaging and physiology measures that have been established as cardiovascular risk markers. (Abbreviations: RWT-relative wall thickness, LV GLS-left ventricular global longitudinal strain, E/e' - ratio of mitral peak velocity of early filling (E) to early diastolic mitral annular velocity (e'), PWV-pulse wave velocity). Please note that thresholds for PWV are age-related. Box plots were derived to display quartiles (Q1, median, Q3) with the upper whisker being Q3+1.5×(interquartile range) and the lower whisker extending to Q1−1.5×(interquartile range) or the lowest data point. **b**, Ultrasound of carotid plaque (6 participants out of 35 had an ultrasound finding of carotid plaque) and relative distribution of ASCVD risk score, HbA1C and LV GLS in function of presence or absence of carotid plaque (Student's *t*-test (two-sided) was used to evaluate differences between groups; $n=35$, 36 measurements) (Abbreviations: CCA-common carotid artery; IJV-internal jugular vein). Error bars represent one standard deviation from the mean (upper edge of box). **c**, Correlation network of selected metrics collected during cardiovascular assessment (Spearman correlation (two-sided) with $q<0.2$; $n=35$ participants with 36 measurements). **d**, Composite *Z* score of ZOBX723 (unstable angina with stent placement) and ZNED4XZ (mild stroke with full recovery and transition to diabetes). For ZOBX723, day 829 occurred 3 weeks post-stent placement. Day 679 was a mid-infection time point. For ZNED4XZ, day 699 was the time point before the participant's transition to diabetes and day 846 was the first diabetic time point. The stroke occurred on day 307 for this individual. Gray dots represent *Z* scores of other participants ($n=101$ with 859 samples). **e**, Violin plot showing the same data as **d** ($n=101$ with 859 samples). The box plot shows the first (lower edge of box), median (middle line) and third (upper edge of box) quartiles. The upper whisker is the third quartile+1.5×(interquartile range) and the lower whisker is the lowest data point.

nature research

Corresponding author(s): Michael Snyder, Francois Haddad

Last updated by author(s): 2/24/2018

Reporting Summary

Nature Research wishes to improve the reproducibility of the work that we publish. This form provides structure for consistency and transparency in reporting. For further information on Nature Research policies, see Authors & Referees and the Editorial Policy Checklist.

Statistics

For all statistical analyses, confirm that the following items are present in the figure legend, table legend, main text, or Methods section.

n/a	Confirmed	
☐	☒	The exact sample size (*n*) for each experimental group/condition, given as a discrete number and unit of measurement
☐	☒	A statement on whether measurements were taken from distinct samples or whether the same sample was measured repeatedly
☐	☒	The statistical test(s) used AND whether they are one- or two-sided *Only common tests should be described solely by name; describe more complex techniques in the Methods section.*
☐	☒	A description of all covariates tested
☐	☒	A description of any assumptions or corrections, such as tests of normality and adjustment for multiple comparisons
☐	☒	A full description of the statistical parameters including central tendency (e.g. means) or other basic estimates (e.g. regression coefficient) AND variation (e.g. standard deviation) or associated estimates of uncertainty (e.g. confidence intervals)
☐	☒	For null hypothesis testing, the test statistic (e.g. *F*, *t*, *r*) with confidence intervals, effect sizes, degrees of freedom and *P* value noted *Give P values as exact values whenever suitable.*
☒	☐	For Bayesian analysis, information on the choice of priors and Markov chain Monte Carlo settings
☐	☒	For hierarchical and complex designs, identification of the appropriate level for tests and full reporting of outcomes
☐	☒	Estimates of effect sizes (e.g. Cohen's *d*, Pearson's *r*), indicating how they were calculated

Our web collection on statistics for biologists contains articles on many of the points above.

Software and code

Policy information about availability of computer code

Data collection	R 3.4 (specified in online methods for which analysis which version was used); HugeSeq, TopHat 2.0.11, HTseq 0.6.1, DESEQ2 v3.5; Perseus v. 1.4.2.40; Progenesis QI (Nonlinear Dynamics); ISEC program;
Data analysis	R 3.5; SAS 9.4; IMPaLA v. 11 (Build April 2018); Cytoscape 3.4.0; R packages: corrplot v. 3.3.2; qvalue v. 1.36.0 in R (v. 3.0.1); Hmisc package (v3.15-0) in R (v 3.0.1); igraph (v.0.7.1); R 3.5 function kmeans; SAS procs: Proc Mixed, Proc Univariate Plot, Proc GAM; QIIME2 with DADA2 denoising plugin; MXM v0.9.7; R v 3.4.1 ridge regression; smartpca tool in the PLINK2 suite; Stringdb v. 10.5

For manuscripts utilizing custom algorithms or software that are central to the research but not yet described in published literature, software must be made available to editors/reviewers. We strongly encourage code deposition in a community repository (e.g. GitHub). See the Nature Research guidelines for submitting code & software for further information.

Data

Policy information about availability of data

All manuscripts must include a data availability statement. This statement should provide the following information, where applicable:

- Accession codes, unique identifiers, or web links for publicly available datasets
- A list of figures that have associated raw data
- A description of any restrictions on data availability

Raw data included in this study are hosted on the NIH Human Microbiome 2 project site (https://portal.hmpdacc.org/) under the study T2D. Data for participants who have not consented to make their data public was deposited into dbGap under accession phs001719.v1.p1.

Field-specific reporting

Please select the one below that is the best fit for your research. If you are not sure, read the appropriate sections before making your selection.

☒ Life sciences ☐ Behavioural & social sciences ☐ Ecological, evolutionary & environmental sciences

For a reference copy of the document with all sections, see nature.com/documents/nr-reporting-summary-flat.pdf

Life sciences study design

All studies must disclose on these points even when the disclosure is negative.

Sample size	Sample size for the main HMP project was calculated based on the pilot iPOP study findings of levels of autocorrelation in multiomics data and the number of timepoints needed per participant to reconstruct the time series with < 1% uncertainty. For this study, we used all iPOP participants with available clinical data.
Data exclusions	All available data was used for analyses. There was no data excluded from analyses.
Replication	This was an observational study which did not involve experiments.
Randomization	Participants were not randomized in this study. There was no allocation to groups, since there is no group-based analysis in the study. In some analyses (mainly mixed effects models involving glucose measures and hsCRP) we controlled for age at time of consent and sex since these covariates were considered potential confounders that could obscure the underlying biological relationships between our omics measures and clinical outcome measures.
Blinding	There was no blinding in this study because it is not relevant to the study (There is no allocation to groups or interventions in the study). Omics data was processed without knowledge of participants' clinical status.

Reporting for specific materials, systems and methods

We require information from authors about some types of materials, experimental systems and methods used in many studies. Here, indicate whether each material, system or method listed is relevant to your study. If you are not sure if a list item applies to your research, read the appropriate section before selecting a response.

Materials & experimental systems

n/a	Involved in the study
☒	☐ Antibodies
☒	☐ Eukaryotic cell lines
☒	☐ Palaeontology
☒	☐ Animals and other organisms
☐	☒ Human research participants
☒	☐ Clinical data

Methods

n/a	Involved in the study
☒	☐ ChIP-seq
☒	☐ Flow cytometry
☒	☐ MRI-based neuroimaging

Human research participants

Policy information about studies involving human research participants

Population characteristics	The mean age of iPOP participants at time of enrollment was 53.4 years old (standard deviation 9.2, range 25-75) and 51% were women. The self-reported ethnic distribution of the cohort was 60% European, 11.9% East Asian, 10.1% South Asian, 6.4% Jewish, 5.5% Hispanic, 5.5% African American, 5.5% Mixed/Other. The most common self-reported health conditions at entry were dyslipidemia (34%) and systemic hypertension (27.5%); participants were generally healthy. Over 78% of the cohort was overweight (BMI between 25 and 30, n = 56) or obese (BMI ≥ 30, n = 28). Our cohort which was enriched for DM risk, had a higher than normal family history of DM (55.0%). Family histories of systemic hypertension (54.1%), coronary artery disease (50.5%) and stroke (23.9%) were also common.
Recruitment	Participants were recruited from the Stanford University surrounding community with the goal of enriching the cohort with individuals at risk for diabetes and thus included individuals who expressed interest in other studies related to diabetes. We do not think the biological results presented are affected by the enriched interest in diabetes studies. However our results related to behavioral change may have more limited generalizability due to the unique characteristics of the Stanford University surrounding community and that there may have been a self selection bias of people interested in intensive monitoring of health which may have impacted their response to such monitoring.
Ethics oversight	Stanford University Institutional Review Board (IRB 23602).

Note that full information on the approval of the study protocol must also be provided in the manuscript.